National University of Science and Technology
Politehnica Bucharest
Faculty of Chemical Engineering and Biotechnologies
Doctoral School Chemical Engineering and Biotechnologies

DOCTORAL THESIS

-Summary-

Spectro-electrochemical studies in the analysis of pharmaceutical compounds

Author:
Eng. Monica-Alexandra Dăescu (Dinescu)

Research Supervisor:
Prof. Dr. Eng. Alina Catrinel Ion

Bucharest, 2024

CONTENT

Keywords: photoluminescence, drug, photocatalytic degradation, composites.

Introduction

The development of the doctoral thesis "Spectro-electrochemical studies in the analysis of pharmaceutical compounds" represents par excellence, an applied activity, combined with a fundamental activity. The application activity aims to create composites based on RGO and TiO2 having anatase-type crystalline structures to improve the efficiency of the degradation of the drug acetaminophenol existing in water resources, respectively the creation of composites based on P5A1N/RGO that may have possible applications in the future that can be used in its detection.

The thesis consists of two parts: part I- synthesis of literature data, which includes chapters 1-4, part II- objectives, apparatus used, experimental part, general conclusions, and novel elements, which includes chapters 5-9.

The first chapter presents information on the chemical and physical properties of active compounds in antipyretic drugs, as well as the theoretical background of the main experimental methods used in the characterization of pharmaceutical compounds.

Chapter 2 outlines the generalities of the degradation processes of antipyretic drugs and the reaction mechanisms that occur in the presence of UV light, pH changes and during hydrolysis reactions.

Chapter 3 provides an overview of TiO_2/RGO catalysts used in the photocatalytic degradation of antipyretic drugs, and Chapter 4 provides an overview of the applications of reduced graphene oxide-based composites functionalized with conducting polymers that are anticipated to be used in the electrochemical detection of antipyretic drugs.

Sections 5 and 6 describe the degradation processes of acetaminophenol and acetylsalicylic acid evidenced by spectral methods.

Chapter 7 presents the synthesis and optical properties of composites based on TiO2 particles and reduced graphene oxide, with applications to the photocatalytic degradation of antipyretic drugs in aqueous matrices.

Chapter 8 describes information on the synthesis and optical properties of composites based on reduced graphene oxide and poly-5-amino-1-naphthol.

The paper concludes with Chapter 9 in which General Conclusions, Elements of Originality and Future Prospects are presented. In the last part of the thesis the dissemination of the experimental results was carried out by publishing scientific papers in peer-reviewed journals, presenting national and international scientific communications and working on patents.

Part II-Original contributions

The critical evaluation of the literature data highlights the importance of drug research in terms of their preparation method, characterization, application in the medical field and their behaviour in contact with the environment. Thus, following these aspects in the research process, the aim of the present thesis is the analysis of antipyretic drugs, as well as the realization and application of TiO_2/RGO, and P5A1N/RGO composites, respectively.

In order to achieve this aim the following objectives will be highlighted:

i) In the first part of the thesis, the photodegradation processes of acetylsalicylic acid and acetaminophen type drugs are explained with the help of photoluminescence (PL). Other techniques for the characterization and identification of pharmaceutical compounds and photodegradation products were Raman scattering, FT-IR spectroscopy and X-ray photoelectron spectroscopy (XPS).

ii) The second section presents the realization of composites based on reduced graphene oxide and titanium dioxide nanoparticles having crystalline structure of anatase and rutile type, to improve the efficiency of degradation of the drug acetaminophen from water samples.

iii) In the third section, the creation of composites based on poly-5-amino-1-naphthol and reduced graphene oxide obtained by cyclic voltammetry was considered, which were characterized by Raman scattering, FT-IR spectroscopy, X-ray photoelectron spectroscopy and atomic force microscopy.

All data obtained in the experimental part of the thesis were recorded using the following types of equipment:

- FT-Raman spectrophotometer, from Bruker, model RFS 100 equipped with YAG (Y3Al5O12):Nd laser allowing the recording of Raman spectra at the excitation wavelength of 1064 nm.
- FTIR spectrophotometer, from Bruker, model Vertex 70 which is equipped with the ATR diamond system.
- UV-VIS-NIR spectrophotometer from Perkin Elmer, model Lambda 950.
- Fluorolog 3-2.2.1 spectrophotometer from Horiba Jobin Yvon, using 90° angle geometry.
- potentiostat/galvanostat from Radiometer Analytical model VOLTALAB 80
- SPECS spectrometer (SPECS Gmbh, Berlin, Germany) using Mg Kα source at 12 Kv and 24 Ma in a vacuum chamber at 2×10^{-8} mbar.
- Nanonics Multiview 4000 microscope (Nanonics Imaging Ltd., Jerusalem, Israel) working in tapping mode in the following conditions: 20 nm probe diameter, 33.08 kHz vibration frequency, 1540 factor of merit and 10 ms/point scan speed.
- SETARAM SETSYS Evolution 18 device in a thermal differential thermogravimetry analyser (TG-DTA, SETARAM Instrumentation, Caluire, France) from room temperature up to 800°C.Zeiss Gemini 500 field emission electron microscope equipped with a Bruker EDS detector.

Chapter 5. Degradation of acetaminophenol (AC) by spectral methods

Chapter 5 describes the raw materials used in the experimental part, as well as the method of obtaining the studied compounds like the fact that AC and NaOH were purchased from Sigma Aldrich. Medicines containing AC as an active compound, marketed as Paracetamol (Magistra C&C), Parasinus (Europharm) and Pararemin (Polisano) were purchased from a local pharmacy. The characterization methods used were: photoluminescence, Raman scattering, IR spectroscopy and XPS spectroscopy. With the help of these methods, the photodegradation processes of acetaminophenol (AC), as well as the interaction of AC with NaOH, were highlighted.

5.2. Optical processes illustrating the controlled degradation of acetaminophen

Study carried out by optical procedures such as Raman scattering, IR absorption and photoluminescence on the interaction of AC with slightly alkaline aqueous medium (pH 6.4-8) highlights the importance/influence of the pH of the reaction medium on the interaction time in

the presence of UV light. The neutralization reaction that takes place in the presence of NaOH is faster in slightly alkaline medium because hydrolysis is favoured which involves the breaking of the -NH-C- bond with the formation of amine and the formation of sodium acetate salt.

5.2.1. Photoluminescence properties of acetaminophen in the absence and presence of excipients

Photoluminescence measurements made in this subchapter were recorded on samples of acetaminophen without excipients. According to Figure 5.1 a, the PLE spectrum of the aqueous solution of AC shows an intense band with a maximum at 317 nm, which is accompanied by another shoulder at 351 nm that has lower intensity. A significant decrease in the intensity of the band located at 317 nm is observed from 1.17×10^6 to 6.1×10^5 counts/sec when AC is exposed to UV light for 140 min (Figure 5.1 a). As AC interacts with NaOH solutions a shift towards longer wavelengths of the PLE bands of AC is induced from 317 nm (Fig. 5.1 a) to 323 nm (Figure 5.1 b), 329 nm (Figure 5.1 c), 336 nm (Figure 5.1 d) and 338 nm (Figure 5.1 e), respectively. The concentrations of the NaOH solutions used in this case are 10^{-3} M, 10^{-2} M, 10_{-1} M and 0.3 M respectively.

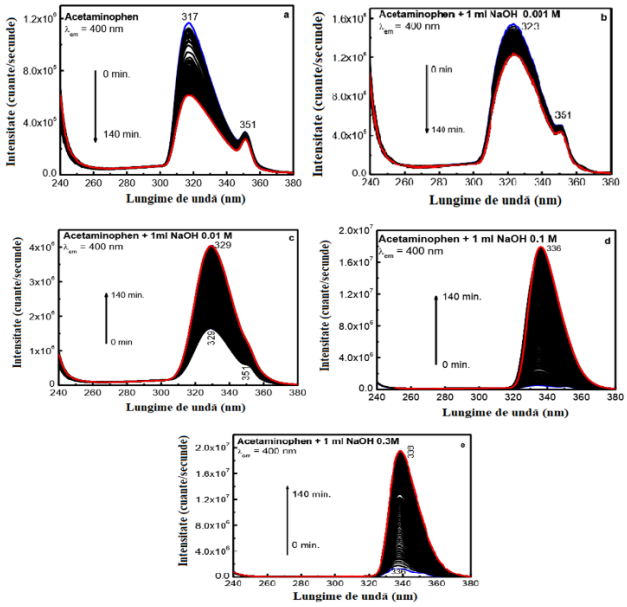

Figure 5.1 PLE spectra of aqueous AC solution before (a) and after interaction with 10^{-3} M (b), 10^{-2} M (c), 10^{-1} M (d) and 0.3 M (e) aqueous NaOH solution. All PLE spectra were recorded at the emission wavelength of 400 nm. The blue and red curves correspond to the first and last PLE spectra of samples exposed to UV light for 0 and 140 min, respectively. The black curves correspond to the intermediate PLE spectra of the above samples, each PLE spectrum being collected at an interval of 84 sec.

Figure 5.2 below highlights the changes in the intensity and position of the AC PL bands when AC interaction with NaOH solutions occurs. The PL spectrum of AC shows two emission bands at 361 and 394 nm, the latter having an intensity equal to 3.3×10^5 counts/sec (Figure 5.2 a). The interaction of AC with NaOH solutions induces an increase in the intensity of the initial PL spectra (blue curves) to aprox. 7.3×10^4 counts/sec, 1.18×105 counts/sec, 1.5×10^4 counts/sec and 1×10^4 counts/sec, respectively. This result can be explained by taking into account the decrease in

the concentration of AC in the reaction mixture with NaOH, leading to the formation of 4-aminophenol and sodium acetate.

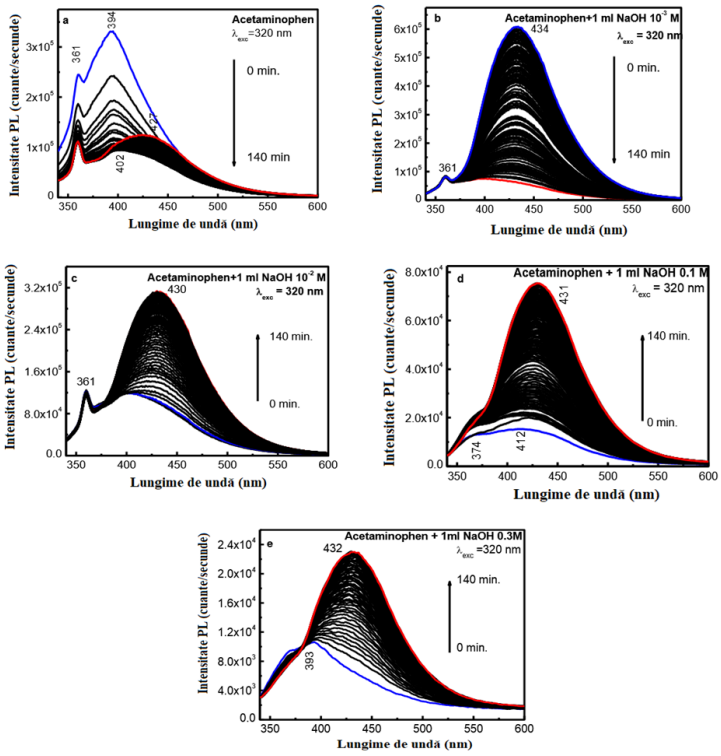

Figure 5.2 PL spectra of aqueous AC solution before (a) and after interaction with 10^{-3} M (b), 10^{-2} M (c), 10^{-1} M (d) and 0.3 M (e) aqueous NaOH solution. All PL spectra were recorded at 320 nm excitation wavelength. The blue and red curves correspond to the first and last PL spectra of samples exposed to UV light for 0 and 140 min, respectively. The black curves correspond to the intermediate PL spectra of the above samples, each PL spectrum being collected at an interval of 140 sec.

PL and PLE studies of AC in the presence of excipients were performed after the filtration process. Figure 5.3, Figure 5.4 and Figure 5.5 show the PLE and PL spectra of the pharmaceutical compounds marketed as Paracetamol, Parasinus and Pararemin before and after their interaction with 0.3 M NaOH aqueous solution. Figure 5.3a shows, the PLE spectrum band of the pharmaceutical compound Paracetamol. The specific maximum of this compound is at 323 nm.

These results confirm that excipients do not influence the evolution of PLE and PL spectra under UV light. The increase in intensity of PLE and PL spectra of AC in the presence of other active compounds and excipients (Figure 5.4, Figure 5.5) is similar to that reported for pure active compounds (Figure 5.1; Figure 5.2). In order to quantify the impact of additional active compounds on AC in the particular case of Parasinus and Pararemin a detailed analysis is required (Figure 5.4 and Figure 5.5), as these drugs contain other active substances in addition to AC, such as chlorpheniramine maleate, pseudoephedrine hydrochloride, propiphenazone and caffeine. In this context, it was found that in the initial state for the two pharmaceutical formulations the PLE band maximum is located at 322 nm, and after their exposure to UV light for 140 min changes in the PLE band intensity of only 4.5% were observed for Parasinus (Figure 5.4 a) and 7.6% for Pararemin (Figure 5.5a), respectively. These values are lower than those reported for AC and paracetamol, where a PLE band intensity change with maxima at 317 nm and 323 nm of 47.8% (Figure 5.1a) and 11.9% (Figure 5.3a) is observed.

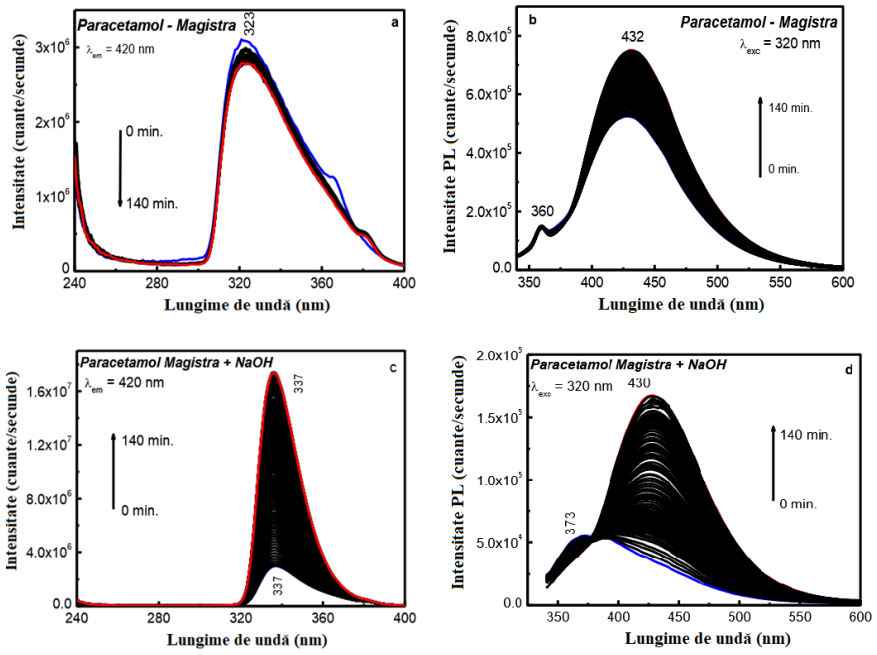

Figure 5.3 PLE and PL spectra of paracetamol aqueous solution before (a, b) and after interaction with 3×10^{-1} M NaOH aqueous solution (c, d). The blue and red curves correspond to the first and last PLE or PL spectra of samples exposed to UV light for 0 and 140 min, respectively. The black curves correspond to the intermediate PLE or PL spectra of the above samples; each PLE and PL spectrum was collected at intervals of 84 sec and 140 sec, respectively.

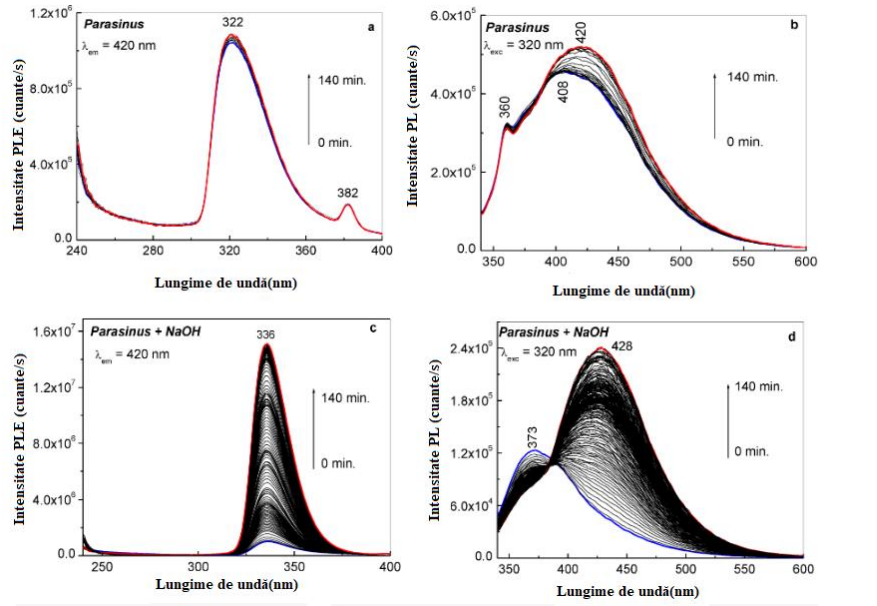

Figure 5.4 PLE and PL spectra of the aqueous solution of Parasinus before (a, b) and after interaction with 3×10-1 M NaOH aqueous solution (c, d). The blue and red curves correspond to the first and last PLE or PL spectra of samples exposed to UV light for 0 and 140 min, respectively. The black curves correspond to the intermediate PLE or PL spectra of the above samples, each PLE and PL spectrum collected at 84 and 140 sec, respectively.

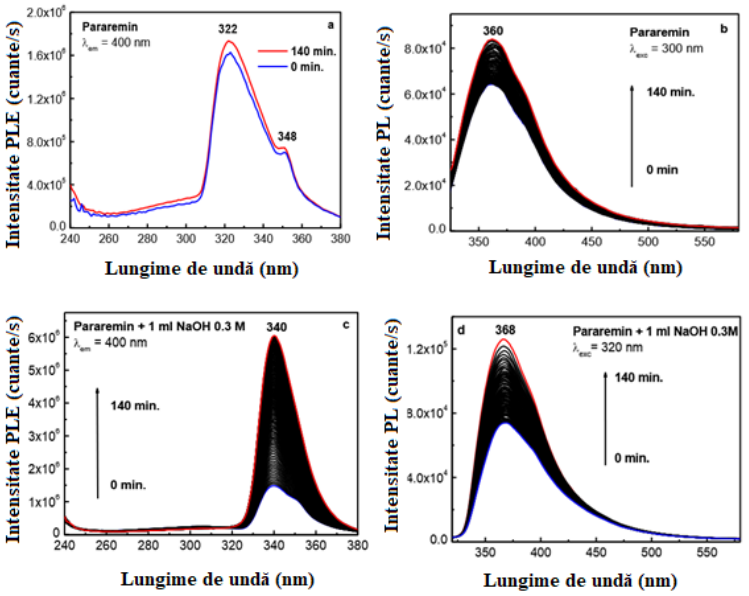

Figure 5.5 PLE and PL spectra of aqueous Pararemin solution before (a, b) and after interaction with 3×10^{-1} M aqueous NaOH solution (c, d). The blue and red curves correspond to the first and last PLE or PL spectra of samples exposed to UV light for 0 and 140 min, respectively. The black curves correspond to the intermediate PLE and PL spectra of the above samples, each PLE and PL spectrum collected at 84 and 140 sec, respectively.

Table 5.1 shows the variations induced in the PL and PLE spectra of AC in the presence of other active compounds and excipients, for the particular cases of Parasinus and Pararemin; the results are shown in Figure 5.4 and Figure 5.5.

Table 5.1. Dependence of the maxima and intensities of the PLE and PL spectra of Parasinus and Pararemin products on UV light exposure time and interaction with NaOH.

Nume medicament	Conc. NaOH (M)	Timpul de expunere lalumina UV (min)	λ_{PLE} (nm)	λ_{PL} (nm)	I_{PLE} (counts/ sec)	I_{PL} (counts/ sec)
Parasinus	0	0	322	408	$1.04x10^6$	$4.55x10^5$
		140	322	420	$1.09x10^6$	$5.22x10^5$
	0.3	0	336	373	$1.02x10^6$	$1.23x10^5$
		140	336	428	$1.5x10^6$	$2.45x10^5$
Pararemin	0	0	322	360	$1.6x10^6$	$6.4x10^5$
		140	322	360	$1.73x10^6$	$8.4x10^5$
	0.3	0	340	368	$1.48x10^6$	$7.36x10^5$
		140	340	368	$6.05x10^6$	$1.27x10^5$

5.2.2 Correlated Raman scattering and IR spectroscopy studies of acetaminophen degradation in the absence and presence of NaOH.

To understand this photodegradation process, when the transformation of the initial acetaminophen occurs during exposure to UV light, correlated IR spectroscopy and Raman scattering studies were performed.Therefore, solid-state samples were used in future experiments

to illustrate the interaction of AC with NaOH. Raman and IR spectra of acetaminophenol are shown in Figure 5.6 and 5.7.

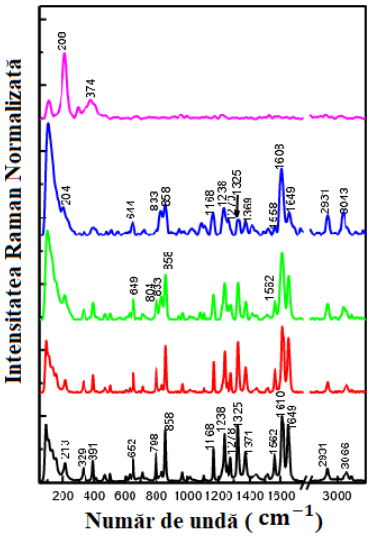

Figure 5.6 Raman spectrum of CA (black curve). The red, green and blue curves correspond to the Raman spectra of AC interacted with NaOH and subsequently exposed to UV light for 140 minutes, when the mass ratio of AC:NaOH is equal to 4.2, 0.5 and 0.4 respectively. The pink curve corresponds to the Raman spectrum of NaOH.

.

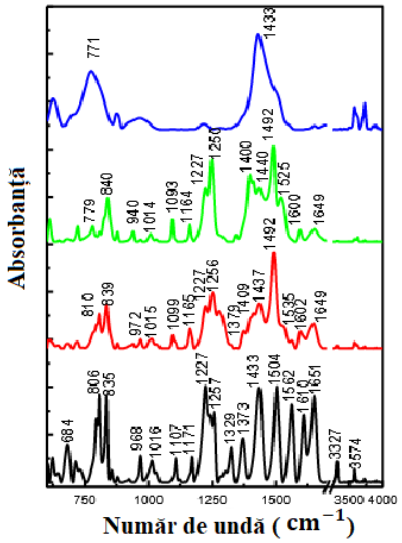

Figure 5.7 IR spectra of AC before (black curve) and after interaction with NaOH, when the AC:NaOH mass ratio is equal to 4.2 (red curve) and 0.4 (green curve), samples were then exposed to UV light for 140 min. The blue curve corresponds to the IR spectrum of NaOH.

5.2.4 XPS studies of acetaminophen in the absence and presence of NaOH

Another characterization technique that has been able to highlight the interaction between AC and NaOH is XPS spectroscopy. XPS spectroscopy measures the kinetic energy of the photoelectrons ejected from the valence electron layer, from which the binding energy specific to each element is obtained, thus the elemental composition of the sample can be revealed. According to the XPS analysis a decrease of the amide group was observed after the AC interaction with NaOH, a process highlighted in Figure 5.9.

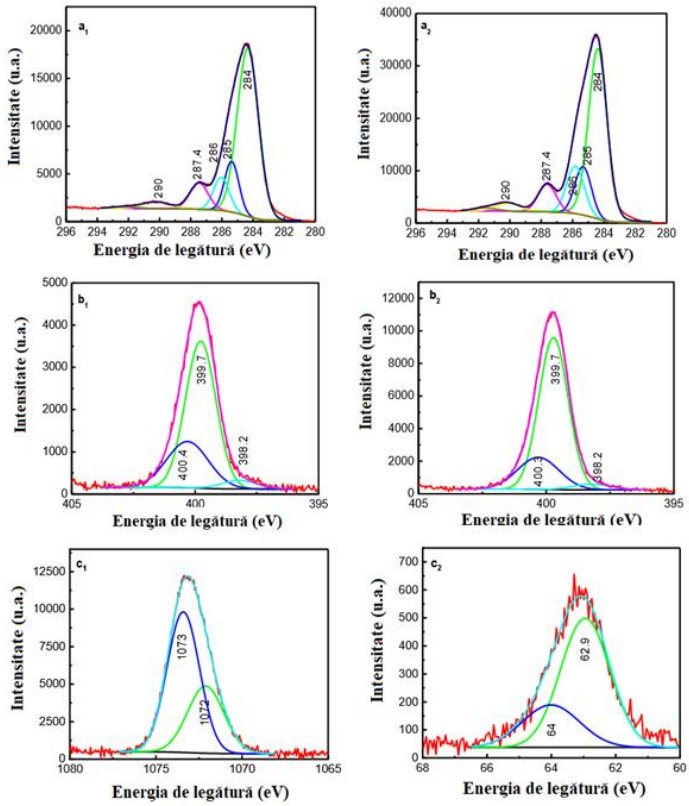

Figure 5.9 XPS C1s (a) and N1s (b) spectra of AC (a1, b1) as well as AC interacted with NaOH (a2, b2). XPS Na1s and Na2s spectra (c1, c2) show AC interacted with NaOH

.

5.3 Partial conclusions

The experimental studies conducted were done taking into account the way acetaminophenol drug is administered with water, which sometimes can have a more basic pH. The risk that may arise from the interaction of AC with aqueous solutions (NaOH solutions) leads to the formation of compounds toxic to the body. In this case, it is p-aminophenol which has high toxic properties. Based on the results presented in this chapter new information on the interaction of AC with NaOH by photoluminescence, Raman scattering and FTIR spectroscopy was revealed. It was thus demonstrated that PL is an alternative method to UV-VIS spectroscopy for monitoring the reaction of AC with NaOH under UV light. In the case of AC interaction with NaOH, a shift of the PLE and PL bands from 317 and 394 nm to 338 and 432 nm, respectively, was reported, simultaneously with an increase in the intensity of these spectra. The PLE and PL studies showed that the AC reaction with NaOH is not influenced by excipients present in pharmaceutical compounds or other active compounds present in antipyretic drugs. The changes observed in the PL spectra were interpreted to be a consequence of AC interaction with NaOH resulting in the formation of p-aminophenol and sodium acetate. The main evidence shown in the Raman spectra for the formation of p-aminophenol and sodium acetate consists of the presence of the Raman line at 1608 cm-1 and the change in the ratio of the relative intensities of the Raman lines at 1649 and 2931 cm^{-1}. The Raman lines at 1608 and 2931 cm^{-1} correspond to the vibrational mode of C=C bond stretching specific to the aniline-derived compound and the carboxyl group, respectively. In the IR spectra, the decrease of the weight of the amide group in AC due to the interaction of AC

with NaOH was evidenced by the absence of the bands located at 1329, 1373 and 3327 cm^{-1}, the decrease of the absorbance of the IR bands located in the spectral ranges 1510-1700 and 3500-3600 cm^{-1} and the presence of the IR band at 1492 cm^{-1} attributed to the vibrational mode of stretching of the C=C bond which is specific to aniline-derived compounds. A decrease of the amide group simultaneously with the formation of amine and carboxyl groups, due to AC interaction with NaOH, was also evidenced by XPS spectroscopy.

Chapter 6. Degradation of acetylsalicylic acid

6.1. Sample preparation methodology.

Acetylsalicylic acid (ASA), $Na2HPO_4$ and NaH_2PO_4 compounds were purchased from Sigma Aldrich. Sodium hydroxide (NaOH) of 98% purity was purchased from Alfa Aesar. Aspirin (ASE) tablets containing 500 mg ASA (active compound) were purchased from local pharmacies. Phosphate buffer (TP) solutions with pH equal to 6.4, 7 and 8 were prepared using aqueous solutions of Na2HPO4 and NaH2PO4. To show the photodegradation of ASA and ASE we prepared an aqueous solution of 0.3 M ASA and another solution of ASE with the corresponding concentration of the active compound ASA of 0.3 M by dissolving an ASE tablet containing 500 mg ASA in 10 mL distilled water or TP, which was then ultrasonicated for 10 min. In order to remove insoluble excipients in the solvent used, successive filtrations were carried out. For hydrolysis reactions of ASA or ASE with alkaline media, aqueous NaOH solutions were 0.3 M

6.2 Optical studies on the degradation of acetylsalicylic acid

Figure 6.1 shows the PLE and PL spectra of ASA and ASE in the solid state. The PLE spectrum of ASA is characterized by an intense band with a maximum at 318 nm and a low intensity band with a maximum at 278 nm, respectively (Figure 6.1a). The ratio of the intensities of these bands reported in the PLE spectrum of ASA is equal to 2.17.

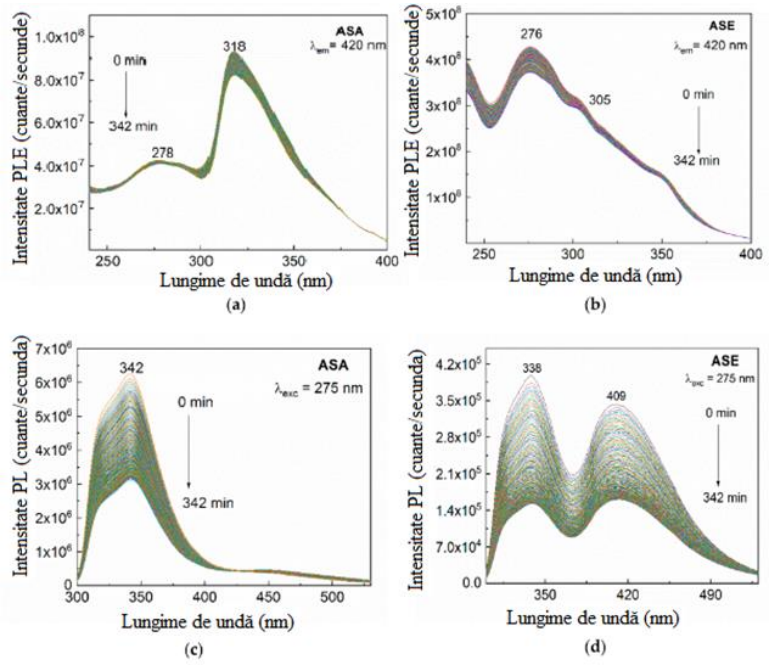

Figure 6.1 PLE spectra of ASA (a) and ASE (b) in powder state recorded at an emission wavelength equal to 420 nm. PL spectra of ASA (c) and pharmaceutical product containing acetylsalicylic acid in the presence of excipients (ASE) (d) in powder form recorded at excitation wavelength equal to 275 nm.

6.2.2 Degradation of acetylsalicylic acid in the presence of H2O and NaOH in the absence and presence of excipients.

The purpose of these photoluminescence measurements in this subchapter was to follow the degradation of aspirin in water. Figure 6.3 shows the degradation of acetylsalicylic acid in the absence and presence of excipients in aqueous solutions. Compared to solid phase samples, aqueous solutions of ASA and ASE showed the following differences before exposure to UV light:(1) the maxima of the PLE and PL spectra of ASA were shifted to 305 nm and 358 nm respectively (Figure 6.3a, b); (2) the PLE spectrum of ASE showed two bands with maxima at 305 nm and 327 nm (Figure 6.3c), and the ratio between the intensities of the two bands located at 305 nm and 327 nm (I_{305}/ I_{327}) became equal to ~ 0.91; (3) The PL spectrum of ASE illustrated an intense band with a maximum at 403 nm, accompanied by a shoulder at 358 nm (Figure 6.3d). The ratio between the intensities of the two bands at 358 and 403 nm (I_{358}/ I_{403}) was equal to 0.48.

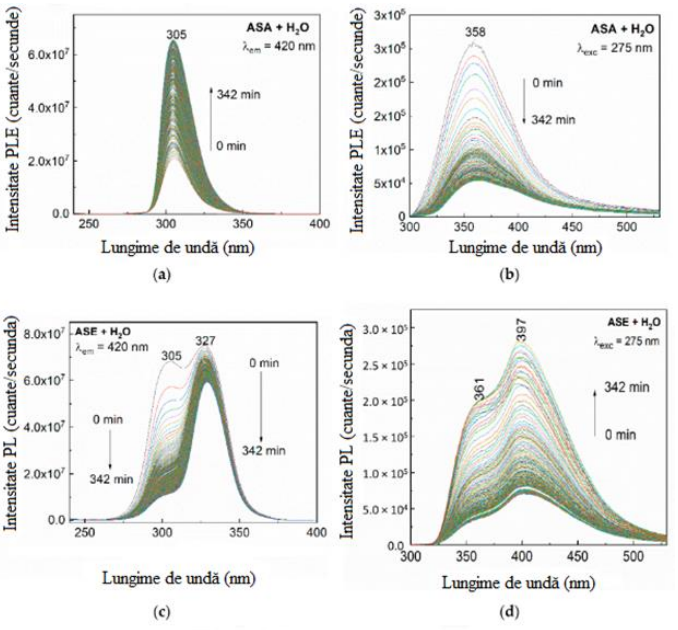

Figure 6.3 PLE and PL spectra recorded at 420 nm emission wavelength and 275 nm excitation wavelength, respectively, of aqueous solution of 0.3 M ASA (a, b) and 0.3 M ASE (c, d).

In the case of ASA samples interacted with NaOH, the following were observed: (i) an increase in the intensity of the PLE spectra from 4.81×10^7 counts/sec to 8.34×10^7 counts/sec, followed by a decrease in intensity to 6.49×10^7 counts/sec. This variation was accompanied by a shift of the PLE band from 306 nm to 319 nm as shown in Figure 6.4a; (ii) a progressive decrease in the intensity of the PL bands from 4.73×10^5 counts/sec to 2.5×10^7 counts/sec (Figure 6.4b). The PLE and PL spectra were recorded at the emission wavelength of 420 nm and the excitation wavelength of 275 nm, respectively, for 342 min.

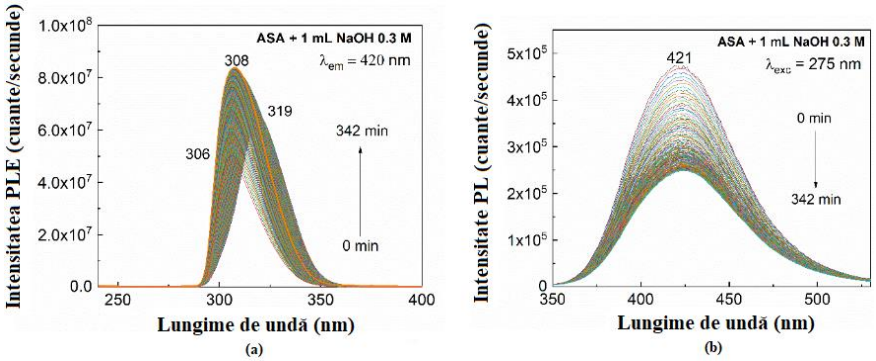

Figure 6.4 PLE and PL spectra of 0.3 M ASA after interaction with 1 mL 0.3 M NaOH (a, b). The volume of the ASA solution was 2 mL.

Similar variations were observed when 0.3 M aqueous ASE solution interacted with 0.3 M NaOH solution..

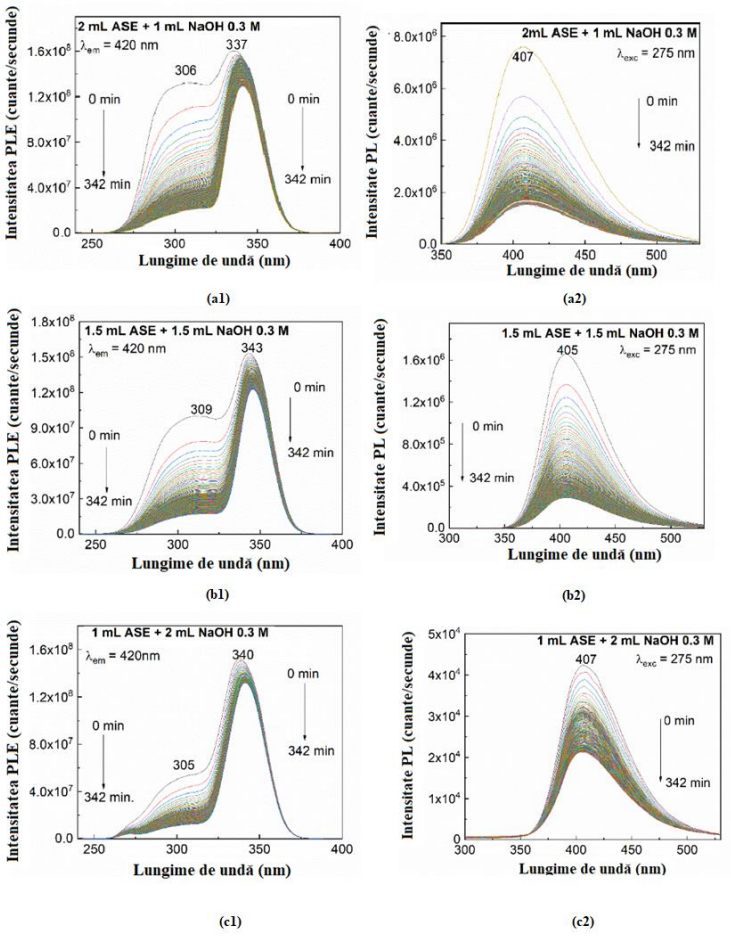

Figure 6.5 PLE and PL spectra of ASE with 0.3 M NaOH in volumetric ratio: 2: 1 (a1, a2), 1.5: 1.5 (b1, b2) and 1: 2 (c1, c2). The PLE and PL spectra were recorded at emission wavelength equal to 420 nm and excitation wavelength equal to 275 nm, respectively.

6.2.3 Influence of pH of phosphate buffer solutions on the degradation of acetylsalicylic acid

Figure 6.7 below shows the dependence of the PLE and PL spectra of ASE on the pH value of the phosphate buffer. The PLE and PL studies performed on these samples at λ_{em} = 420 and λ_{exc} = 275 nm were recorded at room temperature. Analyzing the ASE samples in the presence of TP by means of photoluminescence, changes in the PL and PLE spectra were observed. The changes consisted of a slight shift of the maximum from 332 nm to higher values (338 nm) with pH variation, respectively a decrease in intensity of the band at 302/305 nm from 1.23×10^6 counts/sec (pH=6.4) to 9.55×10^6 counts/sec (pH=7), respectively to 2.05×10^7 counts/sec (pH=8).

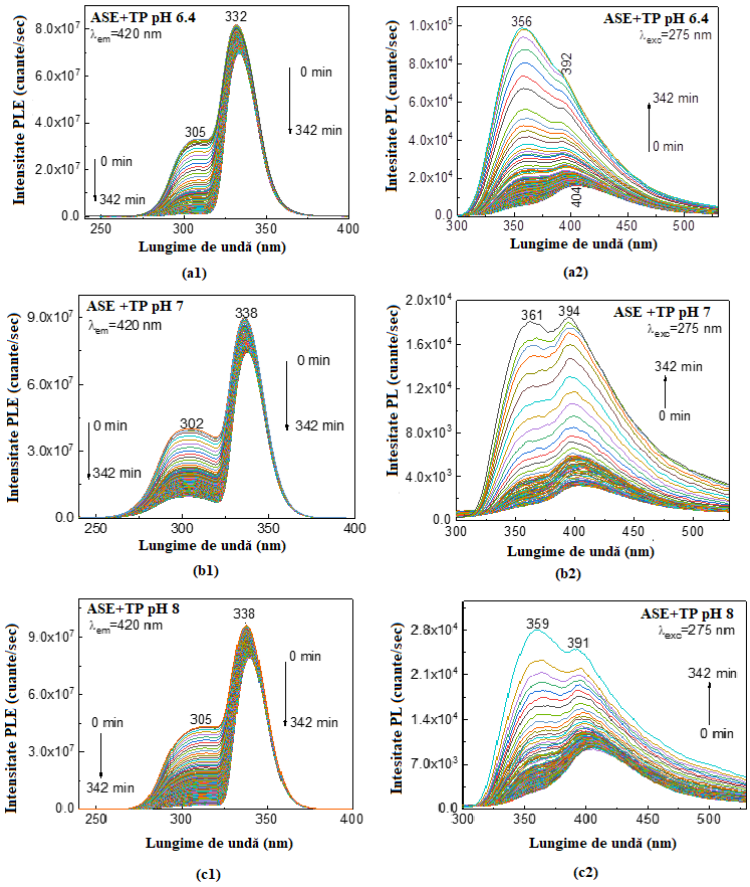

Figure 6.6 PLE and PL spectra of ASE in the presence of TP with pH equal to 6.4 (a1, a2), 7 (b1, b2) and 8 (c1, c2). The PLE and PL spectra were recorded at emission wavelength equal to 420 nm and excitation wavelength equal to 275 nm, respectively.

6.2.4. Correlated Raman scattering and IR spectroscopy studies of acetylsalicylic acid degradation in the absence and presence of NaOH

Figures 6.8 and 6.9 show the Raman and IR spectra of ASA in the initial state and after interaction with NaOH. Figure 6.2.7a shows the Raman spectrum of ASA before interacting with NaOH. Thus, Raman and FTIR spectroscopy measurements revealed the interaction of ASA with NaOH by changing the ratio between the intensities of the Raman lines at 1649 and 2931 cm^{-1}, which were attributed to the vibrational stretching modes of the C=C bond belonging to the aniline and the carboxyl group, respectively, respectively by decreasing the absorbance of the bands

located in the spectral ranges 1510-1700 and 3500-3600 cm^{-1} which are attributed to the amide group, concomitant with the presence of the IR band at 1492 cm^{-1} which is attributed to the vibrational mode of stretching of the C=C bond, belonging to the aniline type compounds.

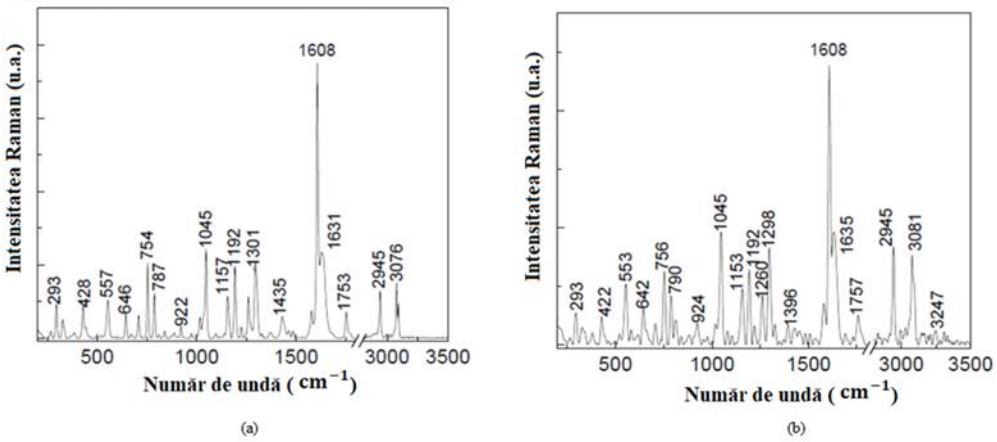

Figure 6.8 Raman spectra of ASA in the initial state (a) and after interaction with NaOH (b) .

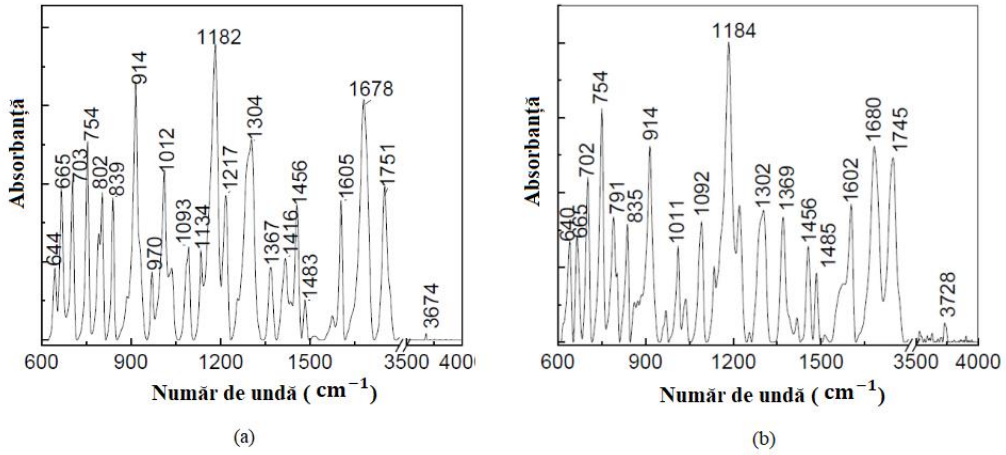

Figure 6.9 IR spectra of ASA in the initial state (a) and after interaction with NaOH (b).

6.2.5 Reversibility of acetylsalicylic acid solution degradation processes induced by temperature variations revealed by photoluminescence studies

In the particular case of aspirin, which is marketed in the form of effervescent tablets, known under the trade names Aspirin Bayer and Aspirin C plus, it is of interest to know the behaviour of this active compound in aqueous solutions. Drinking water is often weakly acidic or basic. Therefore, the aim of this study was to reveal new information on the temperature dependence of PL spectra in aqueous solutions of ASA or ASE (Figure 6.10).

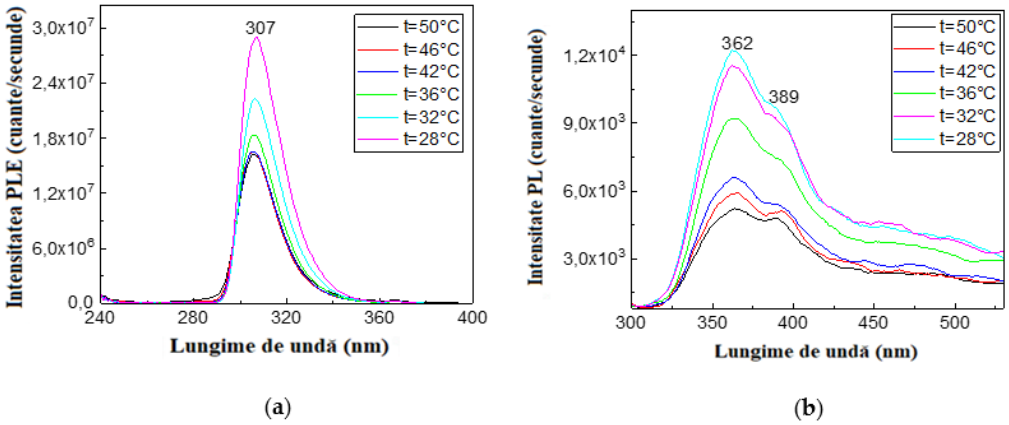

Figure 6.10 Dependence of PLE (a) and PL (b) spectra of 0.3 M ASA aqueous solution on temperature. All PLE spectra were recorded at the emission wavelength of 420 nm, while PL spectra were recorded at the excitation wavelength of 275 nm.

To further argue the degradation processes of ASA occurring in the temperature range 28-50°C, IR spectra of ASA as a function of temperature are shown in Figure 6.11.

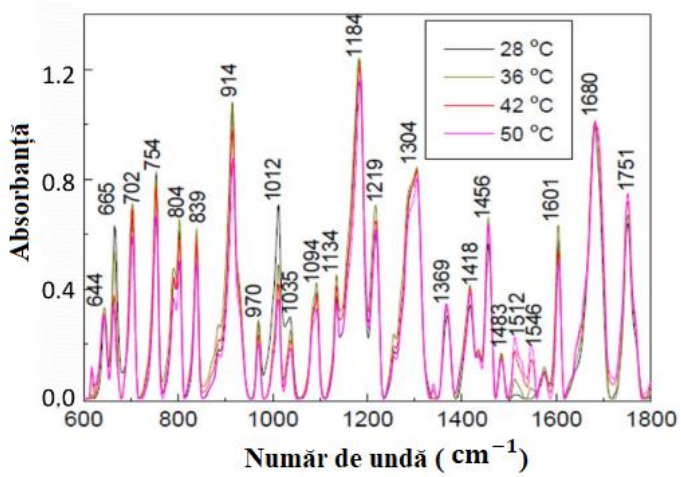

Figure 6.11 Dependence of ASA IR spectra on temperature.

6.4 Partial conclusions

The aim of the experiments carried out in this chapter was to investigate the stability of acetylsalicylic acid (ASA) taking into account its susceptibility to chemical instability through the prism of ester functional groups. Due to these groups, under the influence of light and temperature, in aqueous medium, following the hydrolysis reaction, intermediate compounds such as salicylic acid (SAL), acetic acid, sodium salicylate, sodium acetate are formed from ASA, which in large quantities can be toxic. Photoluminescence spectroscopy was used for in situ monitoring of ASA photodegradation reactions, while Raman scattering and IR spectroscopy were used to highlight the formation of reaction products. Photoluminescence measurements revealed that: i) the presence of SAL in aspirin tablet (ASE) in solid phase is a consequence of partial conversion of ASE to SAL in the presence of water vapour from air adsorbed on the surface of ASE tablets; ii) the hydrolysis reaction of 0.3 M ASA solutions in phosphate buffer medium of pH 6.4, 7 and 8,

induced a gradual increase in the intensity of the PLE spectra of ASE simultaneously with a progressive decrease in the intensity of the PL spectra**;** iii) the hydrolysis reaction of 0.3 M ASA solutions in phosphate buffer medium at pH 6.4, 7 and 8 showed a different behavior due to the presence of SAL and iv) in the particular case of aspirin, which is marketed as effervescent tablets, known commercially as Bayer Aspirin and Aspirin C plus, the PLE and PL spectra of the aqueous ASA solution after the heating-cooling process affirmed an irreversible character, heating favouring the formation of SAL. Raman and IR spectroscopy highlights the interaction of ASA with NaOH by changing the intensity ratio of Raman lines with maxima at 1608 cm^{-1} and 557 cm^{-1} or 2945 cm^{-1}, with the decrease of ester groups in favour of the formation of carboxyl groups specific to the SAL compound.

Chapter 7. Photocatalytic degradation study of antipyretic drugs in aqueous matrices: Degradation of acetaminophen in the presence of catalyst based on reduced graphene oxide and TiO2 with anatase and rutile crystal structure

The aim of this study was to highlight the synthesis of TiO_2/RGO mixtures that occurs through the solid-phase interaction of TiO2 particles with RGO sheets, and their influence in the photocatalytic degradation of acetaminophen. Characterization of TiO_2/RGO mixtures was performed by Raman scattering and FTIR spectroscopy. The photocatalytic properties of TiO_2/RGO mixtures on AC photodegradation in the presence of UV light will also be presented, taking into account the concentration of RGO in the mass of TiO_2/RGO mixtures, the concentration of TiO_2/RGO mixtures as well as the pH of the solution using UV-VIS spectroscopy.

7.2 Optical and structural properties of TiO2/RGO mixtures

Figure 7.1 below shows the main Raman lines of TiO2 located at ca. 147, 405, 447, 523 and 638, 1178, 1205, 1329-1373 -1583-1612 cm^{-1}. In the spectral range 1000-1700 cm^{-1}, the Raman spectrum of RGO shows two bands with maxima at 1292 and 1597 cm^{-1} attributed to the respiratory vibrational mode of the hexagonal rings containing carbon atoms and the phonon E2g mode at the center of the Brillouin zone, respectively [215]. As shown in Figure 7.2.1, the solid-phase interaction of TiO2 with RGO induces a cumulative effect of the vibrational modes of the two constituents of the TiO2/RGO mixture, simultaneously with a shift towards higher values of the D-band from 1292 to 1301 cm^{-1}. The shift of the D-band indicates an increase of the disorder state in the RGO lattice.

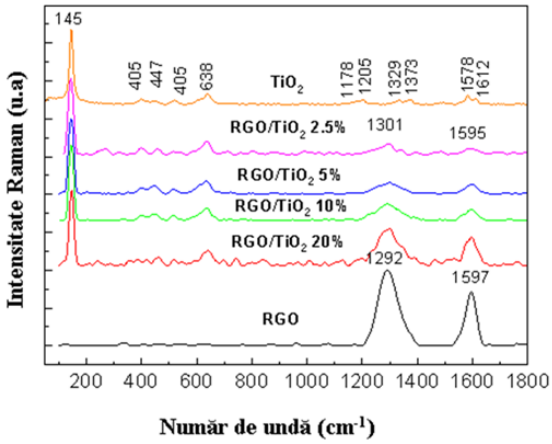

Figure 7.2.1 Raman spectra of TiO_2 particles (orange curve), RGO sheets (black curve) and their mixtures with RGO sheet concentration equal to 5% (blue curve), 10% (green curve) and 20% (red curve).

In addition to the information on the solid phase interaction of TiO_2 with RGO, FTIR spectroscopy measurements were also performed (Figure 7.2). The main IR bands of TiO_2 are located in the spectral range of 500-700 cm^{-1}, which are accompanied by other IR bands with low absorbance peaking at ca. 1382, 1737 and 3627-3728 cm^{-1}. The IR bands whose maxima are located at 692, 1737 and 3627-3728 cm^{-1} are attributed to vibrational stretching modes of the Ti-O-Ti bond, water molecules and vibrational stretching modes of the O-H bond [218]. The interaction of TiO_2 with RGO induced an increase in the absorbance of the IR bands located in the spectral ranges 1000-1800 cm-1 and 3626-3730 cm^{-1}. The increase in the absorbance of IR bands from 1740 cm^{-1} and 3627-3728 cm^{-1} indicates preferential adsorption on the surface of RGO sheets by water molecules existing on the surface of TiO_2 particles.

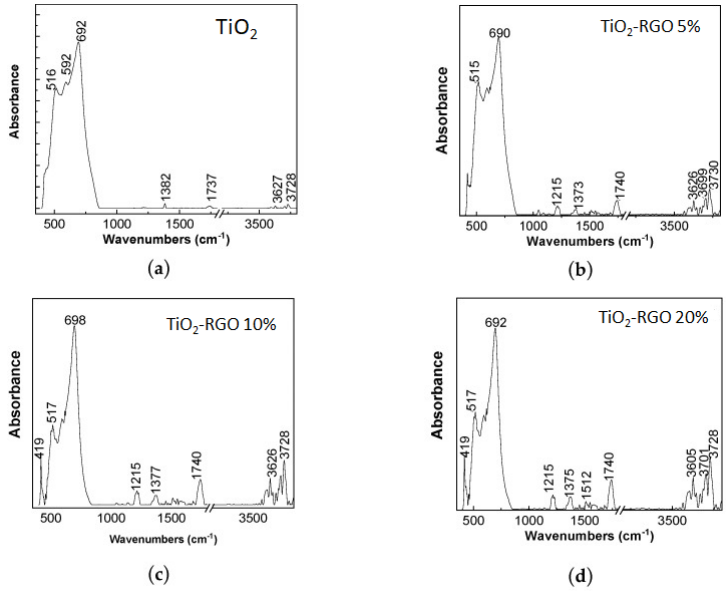

Figure 7.2 IR spectra of TiO_2 particles (a) and mixtures of TiO2 with RGO having RGO sheet concentration equal to 5%, 10% and 20% respectively.

The SEM images shown in Figure 7.3 indicated that the RGO sheets have many wrinkles (Figure 7.3a), and the TiO_2 particle sizes vary in the range 14-317 nm (Figure7.3b). Another aspect that stood out in the SEM figures was the adsorption of TiO_2 particles on the surfaces of RGO sheets, in the case of TiO_2/RGO mixtures with 5% RGO concentration (Figure 7.3c), of TiO_2 particles both on the surfaces of RGO sheets (Figure 7.3d1) and between RGO sheets (Figure 7.3d2), when the RGO concentration in TiO_2/RGO mixtures is 10%, and the presence of a small mass of adsorbed TiO_2 particles on the surfaces of RGO sheets, most of which are covered by RGO layers (Figure 7.3e).

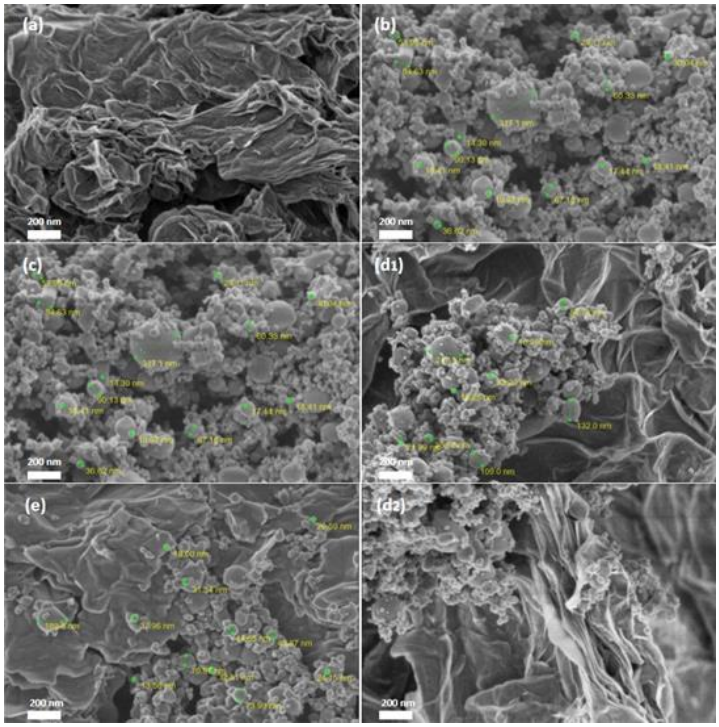

Figure 7.3 SEM images of RGO sheets (a), TiO_2 particles (b) and TiO_2/RGO mixtures with RGO sheet concentrations equal to 5% (c), 10% (d1, d2) and 20% (e).

The EDS spectra of each sample (Figure 7.4) show the presence of Ti, O and C elements in the TiO2/RGO mixtures.

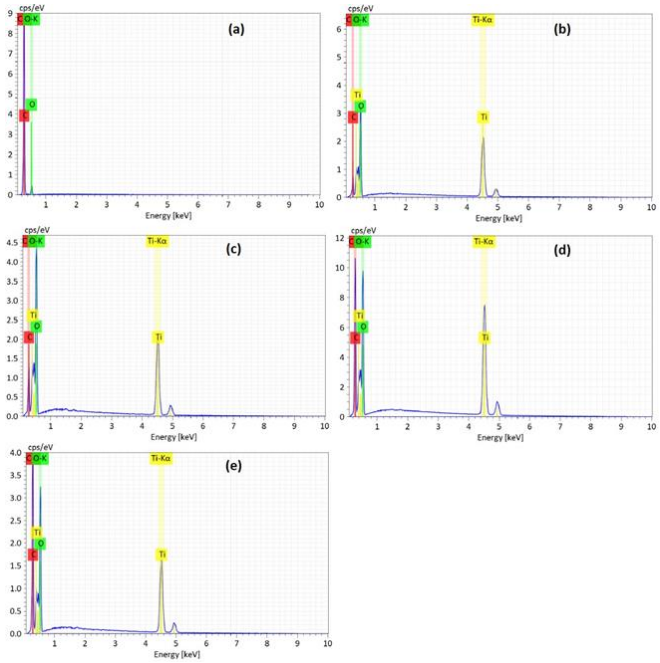

Figure 7.4 EDS spectra of RGO sheets (a), TiO_2 particles (b) and TiO_2/RGO mixtures with RGO sheet concentration equal to 5% (c), 10% (d) and 20% (e).

7.3 Photocatalytic properties of CA in the presence of TiO2/RGO mixtures

The Perkin Elmer UV-VIS-NIR spectrophotometer was used to determine the photocatalytic properties of TiO_2/RGO mixtures in the presence of AC. AC samples in water in the presence of TiO2/RGO were analysed under dark conditions, recording absorption spectra every 5 minutes for 30 minutes until the adsorption/desorption equilibrium of AC on the catalyst surface was reached. During these measurements, no relevant changes in AC absorbance were observed under dark conditions and in the presence of TiO_2/RGO catalyst in the reaction medium. More intense changes were observed when TiO_2/RGO AC samples were exposed to UV light. The photodegradation efficiency of AC in the presence of TiO_2 catalysts and TiO_2/RGO mixtures was calculated with the following equation:

$$D_{eff} = \left(\frac{A_{init} - A_t}{A_{init}}\right) \times 100 \qquad (7.1)$$

where At and A0 are the absorbance values of the band with maximum at 320-338 nm corresponding to UV light exposure times equal to 0 min. and 100 min respectively. In heterogeneous catalysis, adsorption and desorption are essential elementary processes because adsorption activates the decisive chemical bonds of the reactants and desorption removes the reaction products from the surface.

Figure 7.7 shows the UV-VIS spectrum of the ~2 mM aqueous solution of AC in the presence of 0.5 mg TiO_2 and 0.5 mg, 1 mg and 2 mg of TiO_2/RGO mixtures having RGO concentration equal to 5%. The photodegradation efficiency of AC in the presence of TiO_2 is 43.5%.

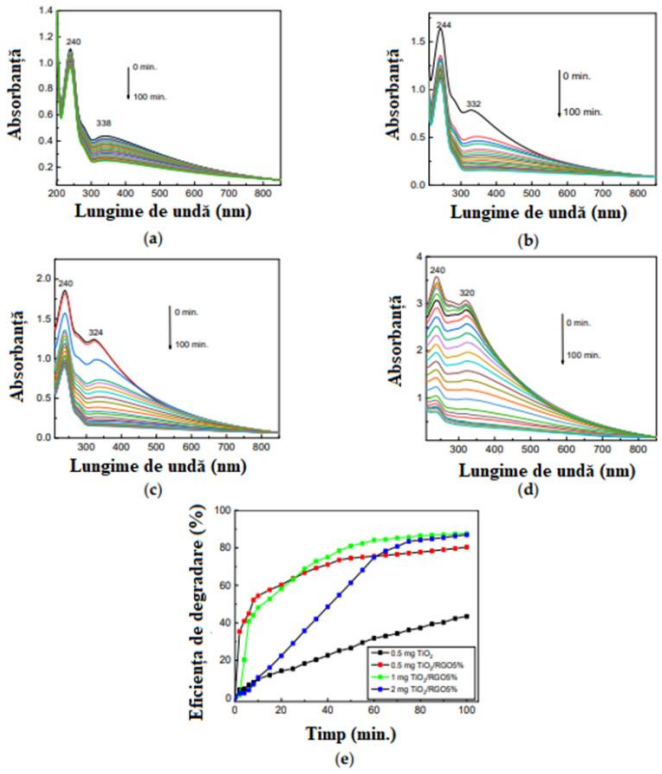

Figure 7.7. Evolution of the UV-VIS spectra of AC in the presence of 0.05 mg/mL TiO_2 (a) and the TiO_2/RGO blends with RGO concentrations of 5 wt% during exposure to UV light for 100 min. The weights of the TiO_2/RGO composites added to the 0.2 mM AC solution were 0.05 mg/mL (b), 0.1 mg/mL (c) and 0.2 mg/mL (d). Degradation efficiency of AC in the presence of 0.05 mg/mL TiO_2 and different weights of TiO_2/RGO blends with an RGO concentration of 5

wt%, i.e. 0.5 mg, 1 mg and 2 mg, dispersed in 10 mL of 0.2 mM AC aqueous solution, after subsequent exposure to UV light (e). 10 mL AC solution was used and the amount of TiO_2 used in the RGO mixtures was 1.9 mg.

Figure 7.8 shows the influence of the concentration of RGO sheets in the mass of the TiO2/RGO mixture. A first aspect observed before exposure to UV light and with increasing concentration of RGO sheets in the mass of TiO_2/RGO mixtures up to 10% and 20%, respectively, was the ratio of absorbance of the bands with maximum at 240-244 nm and 338-320 nm equal to ~1.1 (Fig. 7.8a) and 1.2 (Fig. 7.8b). The second aspect observed after exposure to UV light of 2 mM AC aqueous solution in the presence of TiO_2/RGO blends, where the concentration of RGO sheets is 10% and 20% by mass of TiO_2/RGO mixture (2mg) respectively, when the degradation efficiency was equal to 76.95% and 69.69% respectively (Fig. 7.8c).

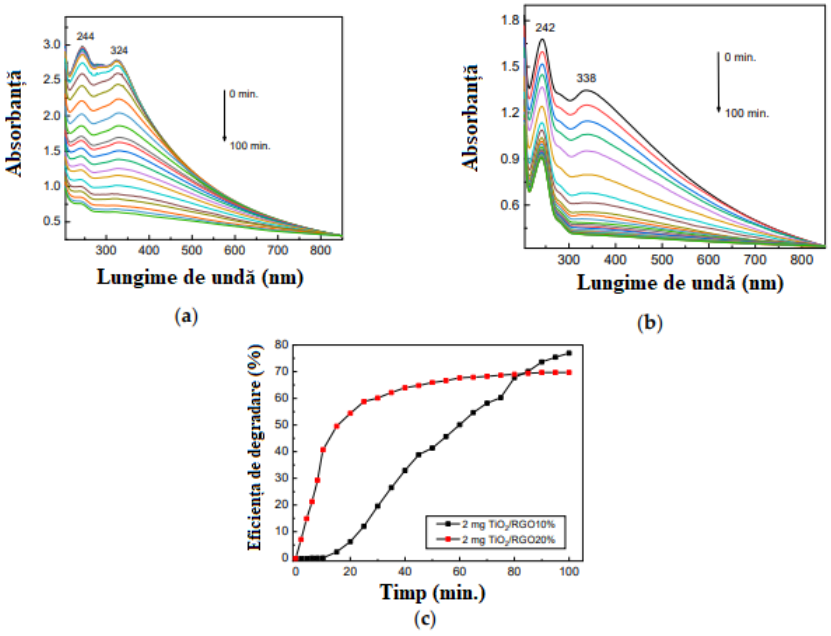

Figure 7.8 Evolution of the UV-VIS spectra of 0.2 mM AC aqueous solution in the presence of 0.2 mg/mL TiO_2/RGO blends with RGO concentrations of 10 wt.% (a) and 20 wt.% (b) when the samples are exposed to UV light for 100 min. Degradation efficiency of AC aqueous solution (0.2 M) in the presence of 0.2 mg/mL TiO_2/RGO blends with RGO sheet concentrations of 10 wt% (black curve) and 20 wt% (red curve) after subsequent exposure to UV light (c).

7.3.2 Evaluation of TiO2/RGO catalyst efficiency as a function of AC solution concentration

Figure 7.9 shows the efficiencies of TiO_2/RGO mixtures with RGO concentrations of 5% with respect to the AC solution with concentrations of 0.1 mM and 0.4 mM. Prior to exposure of the samples to UV light and as the AC concentration was varied from 0.1 mM (Figure 7.9a) to 0.4 mM (Figure 7.9b), there was a hypsochromic shift of the 322 nm band (Figure 7.9a) to 310 nm (Figure 7.9b), which has been attributed to the π-π^* electronic transition of the AC.

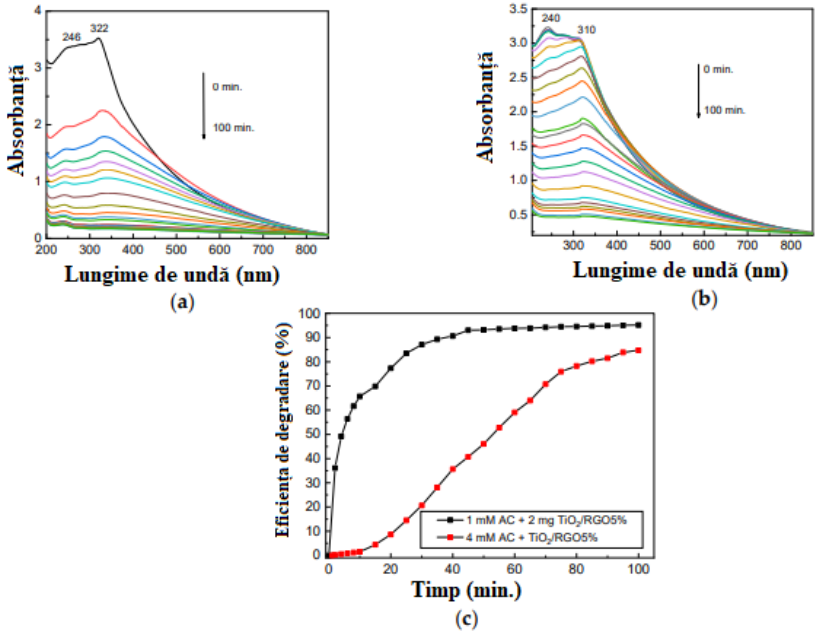

Figure 7.9 Evolution of the UV-VIS spectra of AC in the presence of 0.2 mg/mL TiO_2/RGO blends with RGO concentrations of 5 wt.%, with AC concentrations of 0.1 mM (a) and 0.4 mM (b). Degradation efficiency of AC in the presence of 0.2 mg/mL TiO_2/RGO blends with an RGO concentration of 5 wt.%, when the blends were dispersed in 0.1 mM (black curve) and 0.4 mM (red curve) AC aqueous solution followed by exposure to UV light (c).

According to Figure 7.9c, the photodegradation efficiency of AC solutions with concentrations of 0.1 mM and 0.4 mM in the presence of 0.2 mg/mL TiO_2/RGO mixture with a RGO concentration of 5% was 95.18% and 84.75% respectively. The fourfold decrease in the concentration of the AC solution resulted in an increase of 10.43%.

7.3.3 Kinetic of the AC Photodegradation in the Presence of the TiO2/RGO Blends

The values of the AC photodegradation reaction rate constants for TiO2 and the three TiO_2/RGO mixtures, as well as the linear regression coefficients corresponding to each step are shown in Table 7.1.

Table 7.1. Kinetic reaction constants of aqueous AC solutions in the presence of TiO_2 and TiO_2/RGO mixture having RGO sheet concentration of 5%, 10% and 20%.

Denumirea probei	k_1 (min^{-1})	R_1^2	k_2 (min^{-1})	R_2^2	k_3 (min^{-1})	R_3^2
TiO_2	0.005	0.9979	-	-	-	-
TiO_2/RGO 5%	0.016	0.9943	0.036	0.9959	0.0096	0.9982
TiO_2/RGO 10%	0.040	0.9927	0.0073	0.9899	0.0052	0.9997
TiO_2/RGO 20%	0.0052	0.9869	0.0161	0.9988	0.0168	0.9990

k_1-the generation of the intermediate products caused by the photodegradation of the AC adsorbed onto the TiO_2/RGO blend's surface; k_2-the products resulting from ring cleavage under UV light; k_3- the surface saturation process.

According to Table 7.1, the reaction rate constants show higher values in the case of TiO_2/RGO blends where the concentration of RGO is 5% and 10% compared to TiO_2. Figure 7.3.6 shows the

degradation mechanism of AC in the presence of TiO_2/RGO blends and the chemical reaction of AC with TiO_2/RGO.

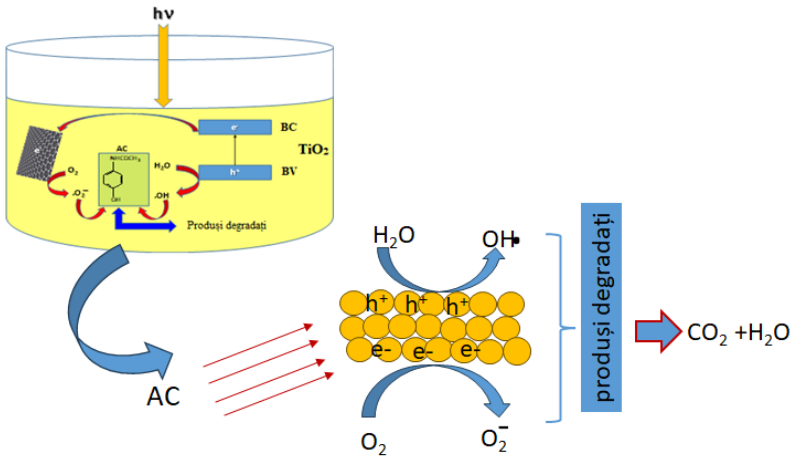

Figure 7.12 Mechanism of AC degradation in the presence of TiO_2/RGO blends.

7.4 The Stability of the TiO_2/RGO Blends

To demonstrate the applicability of TiO_2/RGO mixtures, several cycles of photodegradation of AC were performed, followed by centrifugation to separate the TiO_2/RGO mixture from the aqueous solution. The TiO2/RGO mixture extracted after centrifugation was redispersed in distilled water and then dried at 80°C under vacuum for 30 min. This protocol was also carried out after each AC photodegradation cycle. According to Figure 7.14, when using the TiO2/RGO mixture with 5% RGO concentration in the five photodegradation cycles, a decrease in the AC degradation efficiency from 95.18% to 89.2% was reported. Drying the catalyst at a temperature of 100°C in air for 30 min results in a decrease of the photodegradation efficiency from 95.18% to 91.55%, i.e. only 3.63% (Figure 7.15).

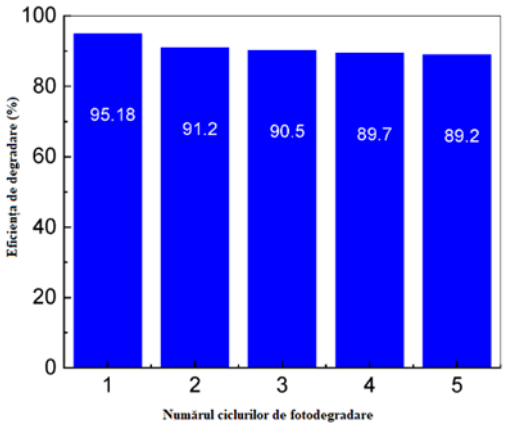

Figure 7.14 Variation in the degradation efficiency of 0.2 mM AC aqueous solution following the reuse of 0.2 mg/mL TiO_2/RGO blend with a concentration of RGO equal to 5 wt. %.

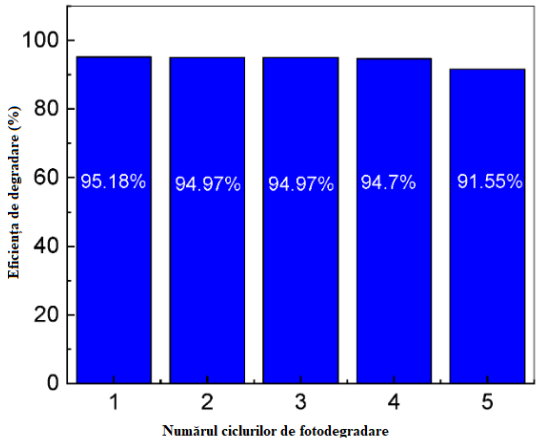

Figure 7.15 Variation in the degradation efficiency of 0.2 mM AC aqueous solution following the reuse of 0.2 mg/mL TiO_2/RGO blend with a concentration of RGO equal to 5 wt. %.

To highlight the performance of the catalyst under real conditions, the TiO_2/RGO mixture was tested in natural water containing 2mg/mL AC. Using the TiO2/RGO mixture with a 5% RGO concentration, the degradation efficiency of 2 mg/mL AC in natural water was only 71.29% (Fig. 7.16).

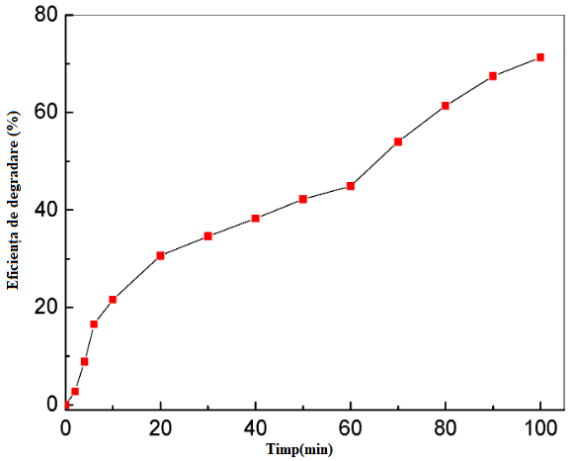

Figure 7.16 Degradation efficiency of 2 mg/mL AC in drinking water in the presence of 0.2 mg/mL TiO_2/RGO blends with an RGO concentration of 5 wt. % after subsequent exposure to UV light.

7.6 Partial conclusions

TiO_2 and TiO_2/RGO photocatalysts were used to improve the degradation of the drug acetaminophenol from polluted water. The catalysts used were obtained by solid phase interaction of TiO_2 particles with RGO sheets. The advantage of using the chemical method through solid phase interaction is the use of a reduced amount of reactants and the efficiency of the preparation time of the TiO_2/RGO samples. The samples obtained were characterised by Raman scattering and FTIR spectroscopy. Using these two characterisation methods, it has been shown that as the concentration of RGO in the mass of the TiO_2/RGO mixture increases, there are i) the shift of the Raman line from 1292 to 1301 cm^{-1}, indicating an increase in the degree of disorder in the graphitic network of RGO; ii) the shift of the IR band, attributed to the Ti-O-Ti vibrational mode, from 692 cm-1 to 698 cm^{-1}, accompanied by an increase in the IR absorption band, with the maximum at

3627-3728 cm^{-1}, attributed to the vibrational stretching mode of the OH bond. The increase in intensity of the IR bands with the maximum at 1737 and 3627-3728 cm^{-1}, respectively, indicates a preferential adsorption of TiO_2 particles on the surface of RGO sheets, facilitated by water molecules adsorbed on the surface of TiO_2 particles. Following the interaction between TiO_2 and RGO, Ti-O-C bonds are formed which favour the photocatalytic process. From a morphological point of view, the TiO_2-RGO samples prepared by the solid phase mixing method appear in the form of TiO_2 flower petals grouped around the RGO sheets, with the TiO_2 particles having sizes in the range of 14-317 nm, depending on the concentration of RGO in the catalyst. The highest AC degradation efficiency, 95.18%, was obtained in the presence of TiO_2-RGO photocatalyst with 5% RGO content.

Chapter 8. Synthesis and optical properties of composites based on reduced graphene oxide and poly(5-amino-1-naphthol) and their applications in the detection of antipyretic drugs

This step presents the synthesis and characterisation of a composite based on reduced graphene oxide (RGO) and poly(5-amino-1-naphthol) (P5A1N). It has been obtained by electrochemical polymerisation of 5-amino-1-naphthol (5A1N) in the presence of perchloric acid ($HClO_4$) and silicotungstic acid ($H_4SiW_{12}O_{40}$), when the working electrode is the Au electrode covered with RGO sheets. The application that can be developed considering this composite is as a platform for detecting the concentration of pharmaceutical compounds in polluted waters.

8.2. Highlighting the chemical interaction of RGO with 5A1N by optical methods

The interaction of 5A1N with RGO sheets induces the following changes in the IR spectra shown in Figure 8. 1, the following changes: (i) a gradual decrease in the absorbance of the IR band from 905 cm^{-1}, accompanied by an increase in the absorbance of the IR band to 3002 cm^{-1} as the concentration of RGO in the 5A1N/RGO mixture increases [229]; and (ii) the appearance of new IR bands with maxima located at 1670 and 3626-3726 cm^{-1}, which have been attributed to the benzene rings and the stretching vibration of the OH bond [232].

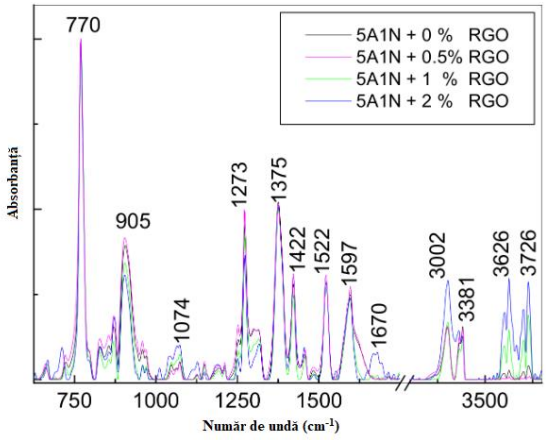

Figure 8.1 IR spectra of 5A1N (black curve) and the 5A1N/RGO mixtures with RGO sheets concentrations equal of 0.5 wt. % (magenta curve), 1 wt. % (green curve) and 5 wt. % (blue curve).

Additional information on the interaction of 5A1N with RGO is provided by Raman spectroscopy (Fig. 8.2).

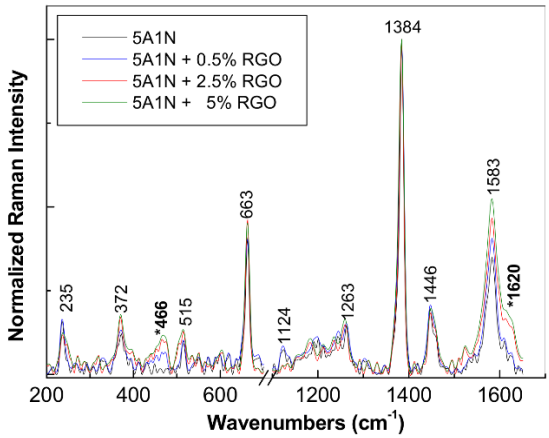

Figure 8.2 Raman spectra of 5A1N (black curve) and the 5A1N/RGO mixtures with RGO sheets concentrations equal of 0.5 wt. % (blue curve), 2.5 wt. % (red curve) and 5 wt. % (green curve).

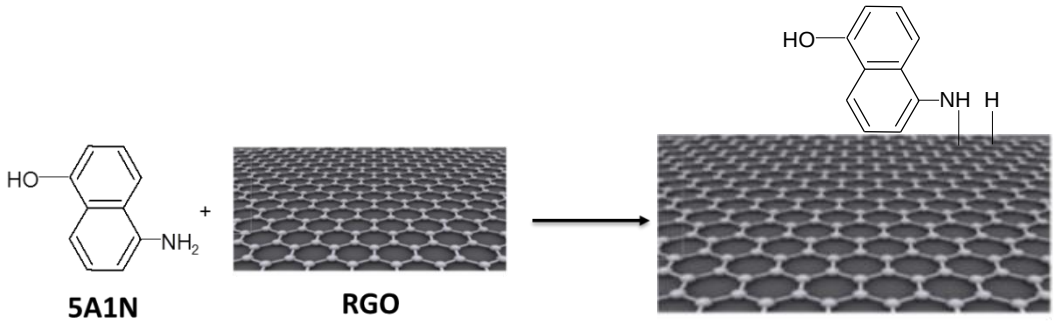

Scheme 8.1 The chemical interaction of 5A1N with the RGO sheets.

In our opinion, Scheme 8.1 can highlight the appearance of IR bands with maxima at 670 and 3626-3726 cm^{-1} as a result of covalent functionalisation of RGO sheets with 5A1N. The appearance of these IR bands corresponds to steric hindrance effects of the aromatic rings and the OH bond originating from 5A1N. Further information highlighting the chemical interaction of 5A1N with RGO sheets is presented below using XPS spectroscopy and thermogravimetric analysis.

8.2.2. Studies by XPS spectroscopy

Figure 8.4 shows the C1s spectra of 5A1N and its composite with RGO. A close analysis of the N1s XPS spectra of 5A1N (Figure 8.4b) and its composite with RGO (Figure 8.4d) shows that the ratio of the intensities of the bands located at 398.9 and 401 eV varies from 5.96 (Figure 8.4b) to 4.84 (Figure 8.4d). Considering this last variation, the decrease of primary amine bonds compared to hydrogen bonds between amine groups can be explained as a result of the transformation of the primary amine functional group into secondary amine groups.

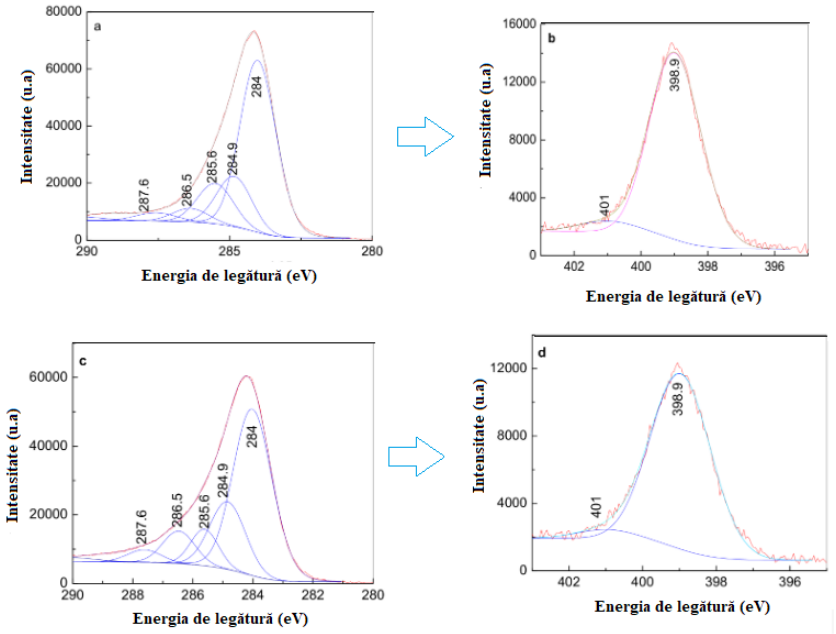

Figure 8.4 XPS C1s spectra of 5A1N (**a**) and the 5A1N/RGO composite (**c**). XPS N1s spectra of 5A1N (**b**) and the 5A1N/RGO composite (**d**).

8.2.3. Differential Thermal and thermogravimetric analysis

Differential thermal and thermogravimetric analysis shows the thermal stability of 5A1N, RGO sheets, and 5A1N/RGO composite (Fig. 8.5).

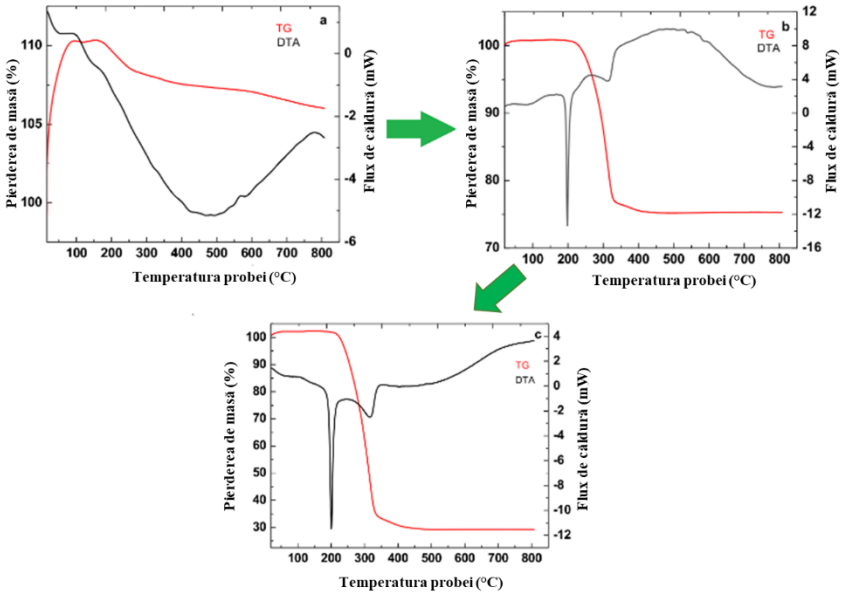

Figure 8.5 TG-DTA curves of the RGO sheets (**a**), 5A1N (**b**) and the 5A1N/RGO composite (**c**).

8.3. Optical characterisation of the electrochemical polymerisation of RGO functionalised with 5A1N

The functionalisation of RGO sheets with P5A1N doped with heteropolyanions of silicotungstic acid $H_4SiW_{12}O_{40}$ was achieved by electropolymerisation of 5A1N on the Au electrode covered with RGO sheets. Cyclic voltammetry studies were performed with the working electrode immersed in a solution consisting of 5A1N (with concentrations between 10^{-3} M, $5x10^{-3}$ M or 10^{-2} M), $H_4SiW_{12}O_{40}$ (with concentrations equal to 10^{-3} M, $5x10^{-3}$ M or 10^{-2} M) and HClO4 0.1 M. The potential range used to record the cyclic voltammograms was between 0 and + 750 mV with respect to the reference electrode (saturated calomel electrode (SCE)). Different potential scan rates of 100, 50, 40, 30, 20, 10, 5 and 2 mV/s were used for these studies.

8.3.1. Cyclic voltammetric studies and reaction mechanisms during electrochemical polymerisation of monomer in the absence and presence of RGO

Figure 8.6 shows the cyclic voltammograms recorded during the electrochemical polymerisation of 5A1N on the Au electrode and on the Au wafers covered with RGO sheets.

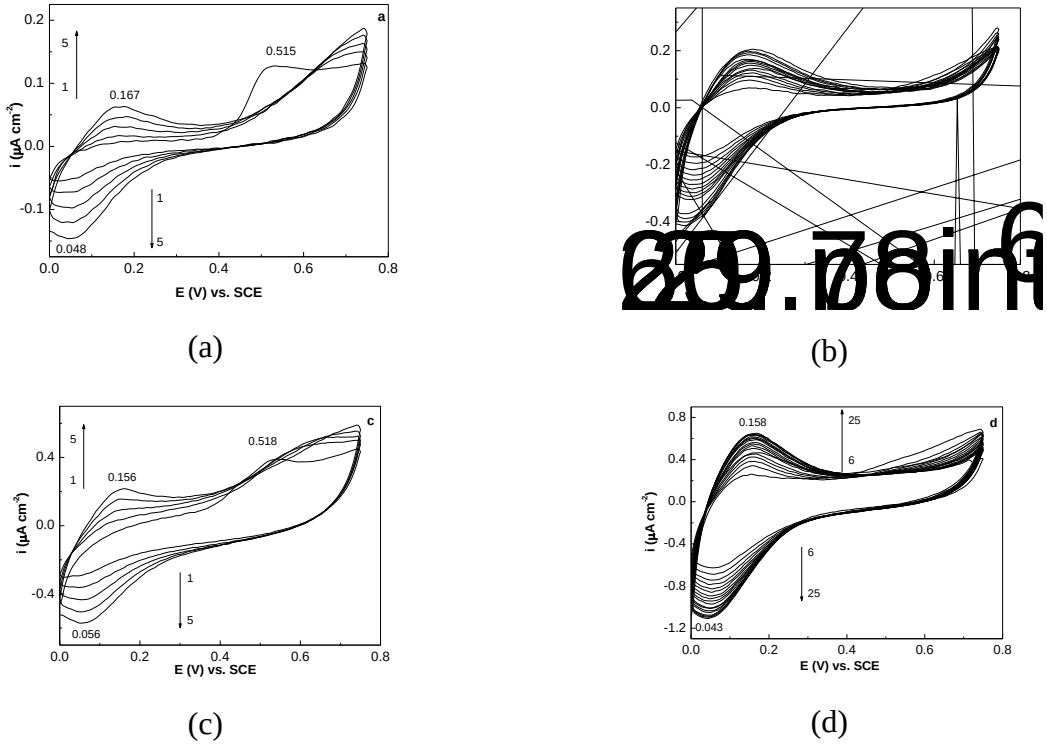

Figure 8.6 The first 1–5 and 6–25 cyclic voltammograms recorded during the electrochemical polymerization of 5×10^{-3} M 5A1N in the presence of 0.1 M $HClO_4$ and 10^{-3} M $H_4SiW_{12}O_{40}$ when the working electrode is the blank Au electrode (a,b) and the Au electrode is covered with the RGO sheets (c,d). The scanning rate is equal to 50 mV s^{-1}.

As can be seen in Figure 8.6, regardless of the number of cyclic voltammograms, the ratio of the current densities of the cathodic and anodic peaks (i_{pa}/i_{pc}) is not equal to unity. All these changes indicate that irreversible processes are taking place at the electrode-electrolyte interface. According to Figure 8.7, for both the Au electrode and the Au plate covered with RGO sheets, it is observed that as the concentration of 5A1N increases, there is an increase in the current densities

in the cyclic voltammograms. This fact indicates a dependence of the rate of the electrochemical polymerization reaction on the concentration of 5A1N.

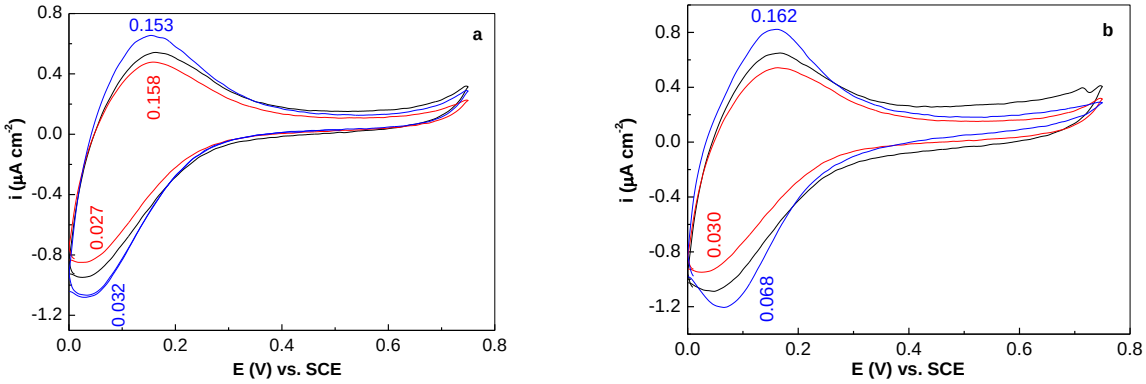

(a) (b)

Figure 8.7 The 25th cyclic voltammogram recorded on the Au electrode (a) and the Au electrode covered with the RGO sheets (b), when the synthesis solution consists of 0.1 M $HClO_4$, 10^{-3} M $H_4SiW_{12}O_{40}$ and 5A1N with the concentration 10^{-3} M (red curve), 5×10^{-3} M (black curve) or 10^{-2} M (blue curve), the scanning rate being equal to 50 mV s^{-1}.

Regardless of the type of working electrode used, both the Au electrode and the Au electrode covered with RGO sheets, it is observed that as the concentration of H4SiW12O40 increases, there is an increase in the current densities of the cyclic voltammograms (Figure 8.8 a, b).

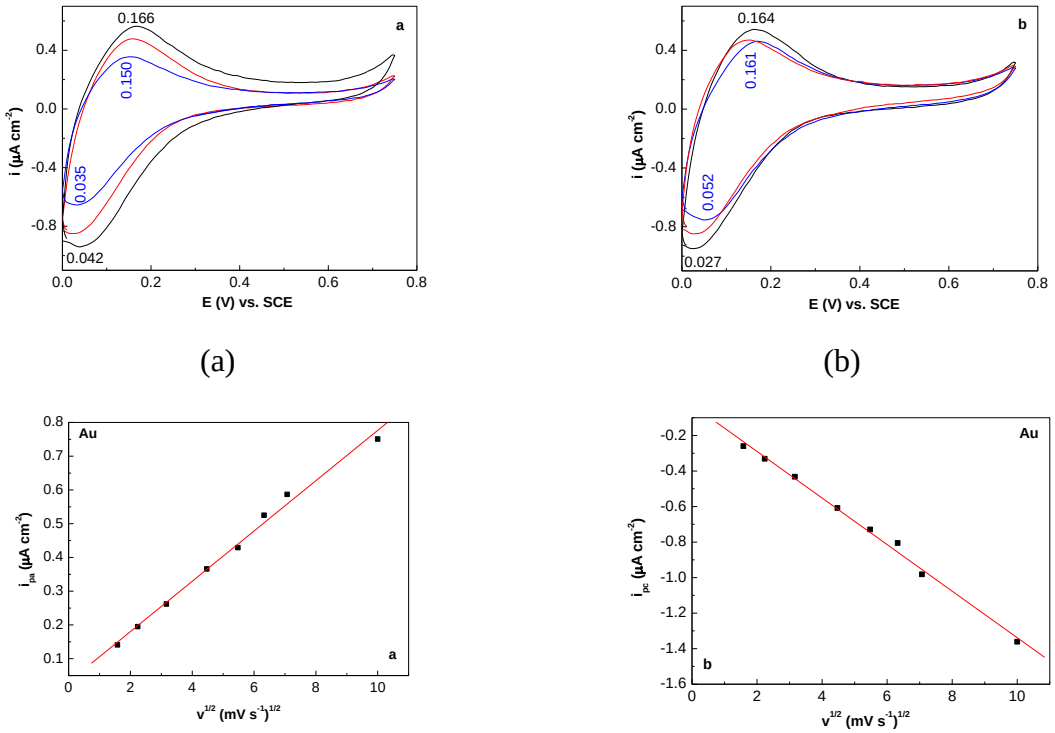

(a) (b)

(c) (d)

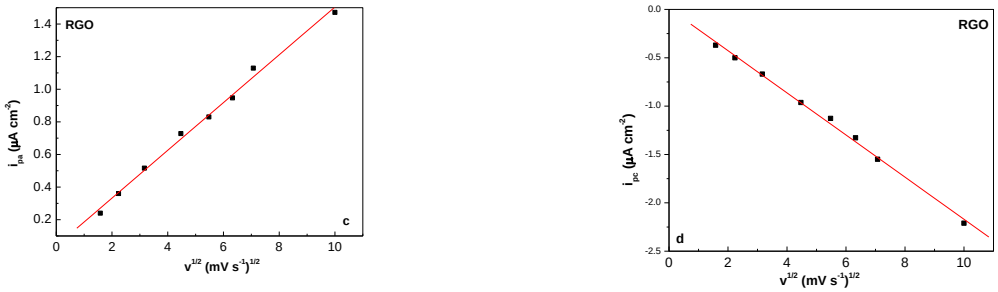

(e) (f)

Figure 8.8 The 25th cyclic voltammogram recorded on the blank Au electrode (a) and the Au electrode covered with the RGO sheets (b), when the synthesis solution consisted of 0.1 M HClO4, 5×10^{-3} M 5A1N and $H_4SiW_{12}O_{40}$ with the concentration 10^{-3} M (blue curve), 2×10^{-3} M (red curve) or 4×10^{-3} M (black curve), respectively , at a scanning rate of 50 mV s^{-1}. The dependence of the current densities of the anodic and cathodic peaks on the scan rate used during the 5th cyclic voltammogram recorded on the blank Au electrode (c,d) and the Au electrode covered with the RGO sheets (e,f), when the synthesis solution consists of 10^{-2} M 5A1N, 0.1 M HClO4 and 2×10^{-3} M $H_4SiW_{12}O_{40}$.

8.3.2 Evaluation of P5A1N/RGO film thickness by AFM studies

The film thickness of P5A1N/RGO was investigated by AFM analysis. As shown in figure 8.9, the Au layer is very smooth, characterized by the decrease of the roughness parameters: 1.5 nm RMS and 1.1 nm Ra. The deposition of RGO sheets on the surface of the Au electrode induces an increase in the roughness parameters to 17 nm RMS and 13 nm Ra. The height of the RGO layer was 60 nm, which was calculated from the AFM image.

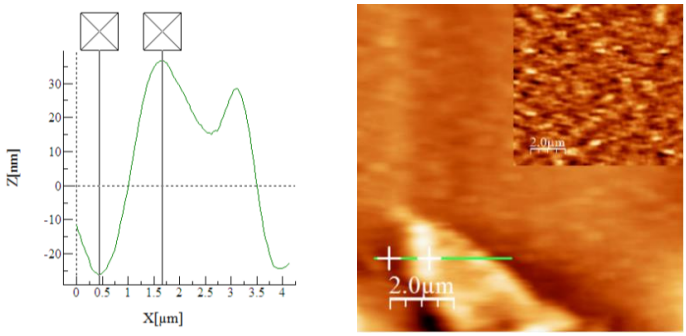

(a) (b)

Figure 8.9 The height of the RGO sheet on the Au electrode (**a**) and Atomic Force Microscopy (AFM) images of the blank Au electrode (insert in b) and the Au electrode covered with the RGO sheets (**b**).

8.3.3. Elucidation of the functionalization mechanism of RGO with P5A1N by correlated Raman scattering and IR spectroscopy studies

Further information on the deposition of P5A1N on the bare Au electrode and on the Au electrode coated with RGO sheets is presented below using IR spectroscopy and Raman scattering. The FT-Raman analysis revealed the characteristic lines of the P5A1N polymer electrosynthesised on the Au electrode as well as the P5A1N polymer electrosynthesised on the Au electrode covered with RGO sheets (Fig.8.10).

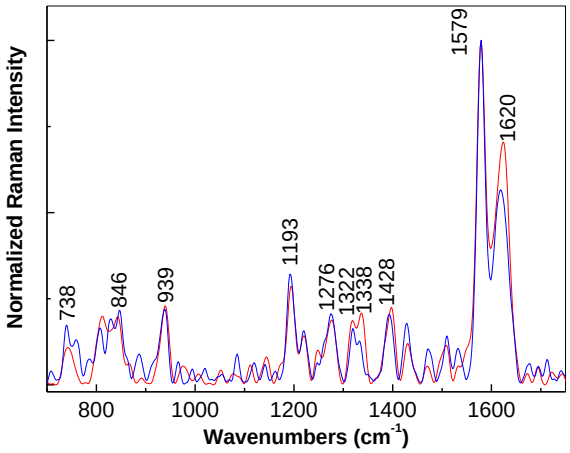

Figure 8.10 he Raman spectrum of P5A1N electrosynthesised on the blank Au electrode (blue curve) and the Au electrode covered with the RGO sheets (red curve).

Other vibrational changes observed in the case of P5A1N electrosynthesised on the Au electrode and on the Au electrode covered with RGO sheets are further reported by IR spectroscopy. In this context, Figure 8.11a highlights the main IR bands of P5A1N synthesised in the presence of $HClO_4$ and $H_4SiW_{12}O_{40}$ on the Au electrode.

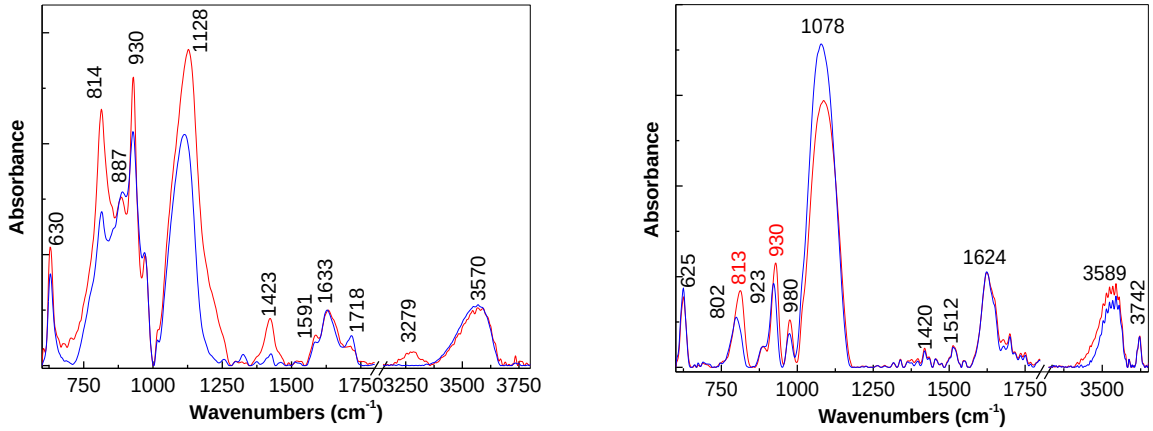

Figure 8.11 The IR spectra of P5A1N electrochemically synthesised onto the blank Au electrode (a) and the Au electrode covered with the RGO sheets (b) by recording 5 (blue curve) and 25 (red curve) cyclic voltammograms.

8.3.4. Potential of RGO/P5A1N composites in electrochemical detection of antipyretic drugs – chemical mechanisms

The presence of this additional bond in the case of P5A1N electrosynthesized on RGO sheets can only be explained by considering the electrochemical polymerization mechanism shown in Scheme 8.2. According to Scheme 8.2, the reaction product of the electrochemical polymerization of 5A1N on the Au electrode covered with RGO sheets consists of RGO sheets covalently functionalized with P5A1N doped with the heteropolyanions $H_4SiW_{12}O_{40}$.

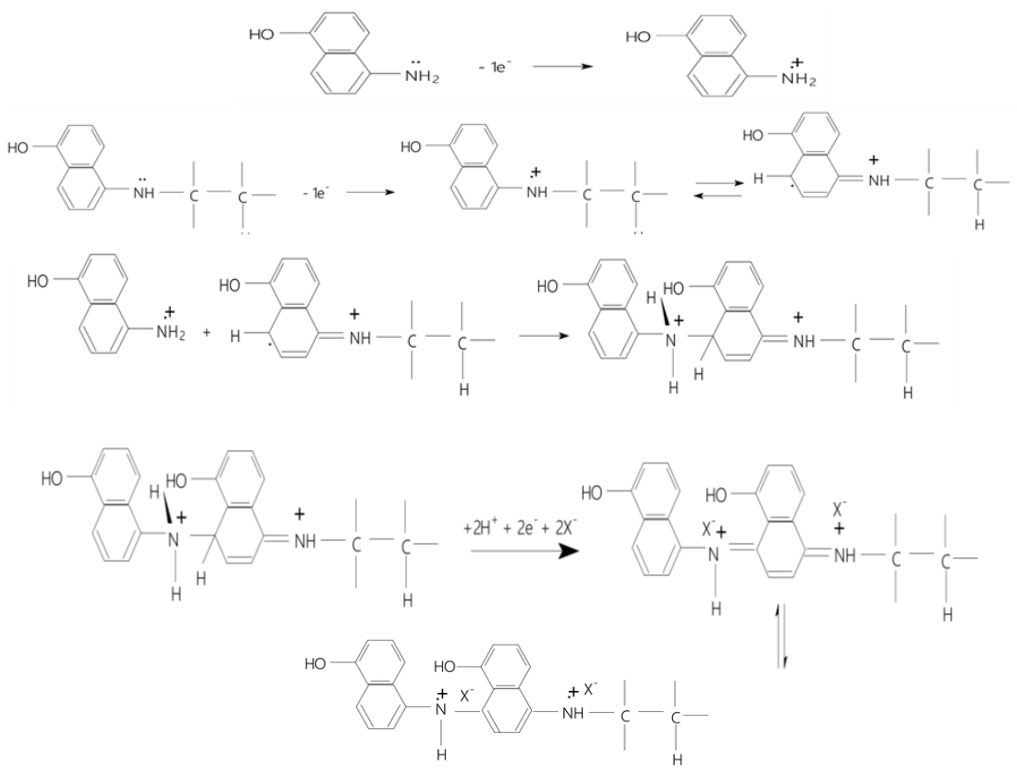

5A1N Dimer covalently functionalized with RGO

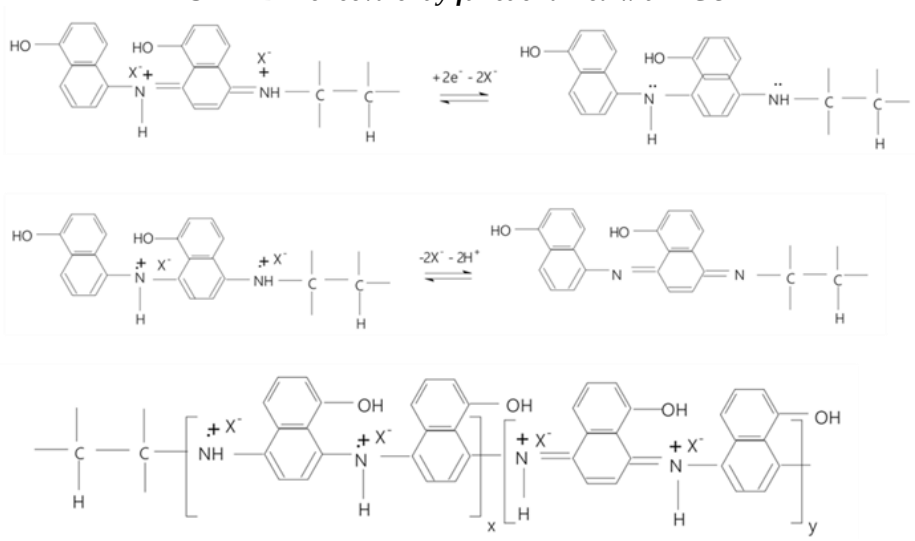

***The RGO sheets covalently functionalized with P5A1N doped with* H4SiW12O40 heteropolyanions**

Scheme 8.2 The mechanism of the electrochemical polymerization of 5A1N in the presence of the RGO sheets, X− corresponds to the $H_4SiW_{12}O_{40}$ heteropolyanions; i.e., $H_3SiW_{12}O_{40}$−. In this scheme, x and y correspond to the numbers of the reduced and oxidized entities of repeating units of macromolecular compound.

Based on the mechanism described above, the RGO/P5A1N composite was used in the realisation of the acetaminophen detection sensor. It can be used to identify the optimum analyte concentration. Figure 8.12 shows the schematic representation of the AC detection sensor.

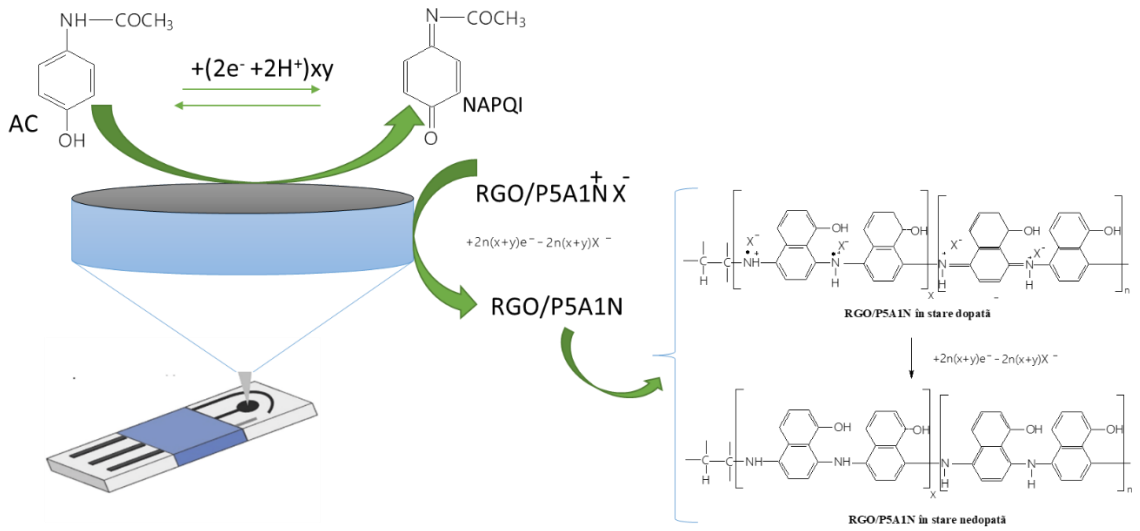

Figure 8.12 Schematic representation of the AC detection sensor.

Chapter 9. General conclusions

The main objectives of this work are the study of the degradation processes of antipyretic drugs in different aqueous environments under the influence of light, as well as the preparation of TiO_2/RGO and RGO/P5A1N type composites, used, on the one hand, for the degradation of pharmaceutical compounds present in wastewater, such as acetylsalicylic acid and paracetamol, and, on the other hand, for the realization of a platform for the detection of the concentration of pharmaceutical compounds. The drugs used in this study were acetylsalicylic acid and paracetamol.

The first part briefly describes the concepts and data from the specialized literature related to the topic of the thesis, and the second part presents the original results obtained in the studies carried out during the doctoral internship.

The second chapter of the second part (**chapter 5**) describes the raw materials used in the experimental part, as well as the method of obtaining the compounds studied. The characterization methods used were: photoluminescence, Raman scattering, UV-VIS and IR spectroscopy and XPS spectroscopy. These methods were used to highlight the photodegradation reactions of acetaminophenol (AC). At the excitation wavelength of 320 nm, a PL band in the spectral range of 340-550 nm was highlighted, the intensity of which decreases as the AC is exposed to UV light. It was also observed that as AC interacted with NaOH solutions at different concentrations, there was an increase in the intensities of the photoluminescence excitation (PLE) and PL spectra. Increasing the exposure time of the samples to UV light up to 140 minutes resulted in the formation of p-aminophenol and sodium acetate. The PLE and PL studies carried out showed that this behavior of AC in UV light is not influenced by excipients or other active ingredients in the drugs. Experimental evidence for the formation of p-aminophenol and sodium acetate when AC interacts with NaOH was presented using Raman and FTIR spectroscopy.

Chapter 6 provides information on the raw materials used in the degradation of acetylsalicylic acid and the drug aspirin containing this type of active ingredient. The techniques used to monitor the degradation of ASA were: photoluminescence, Raman scattering and IR spectroscopy.

The main conclusions of these studies, which are presented in chapters 5 and 6, are that:

- Photoluminescence is a method that can be successfully used to monitor the photodegradation of pharmaceutical compounds such as aspirin and paracetamol, but also to evaluate the behavior of the pharmaceutical product containing aspirin and paracetamol in the presence of alkaline solutions;
- IR absorption spectroscopy, Raman spectroscopy and X-ray photoelectron spectroscopy (XPS) studies were carried out to understand the photodegradation and transformation process of the parent drug during exposure to UV light.

Chapter 7 presents data on the photocatalytic activity of mixtures based on TiO_2 nanoparticles and reduced graphene oxide for the degradation of acetaminophen. The TiO_2/RGO mixtures were prepared by solid phase interaction of TiO_2 particles with RGO sheets. Compared to other reported synthesis methods for TiO_2 and RGO catalysts, the advantages of this method are due to the small number of reactants and the short preparation time of the TiO_2/RGO samples, respectively. In order to highlight the vibrational changes induced by the solid phase interaction of the two components, the characterisation of the TiO_2/RGO mixtures was carried out by Raman scattering and FTIR spectroscopy. The morphology of TiO_2 particles and TiO_2/RGO blends was determined by scanning electron microscopy (SEM). The characterisation of TiO_2 particles, RGO sheets and TiO_2/RGO blends was performed by X-ray photoelectron microscopy. The photocatalytic properties of TiO_2/RGO blends with respect to AC photodegradation in the presence of UV light were carried out taking into account the influence of the amount of RGO in the TiO_2/RGO mixture, by the concentration of the TiO_2/RGO mixtures, as well as by the presence of excipients. The effects of the TiO_2/RGO mixtures on AC degradation as a function of AC solution concentration and in real samples were also presented. In order to demonstrate the performance of the catalyst under real conditions, the TiO_2/RGO mixture was tested in drinking water containing 2 mg/mL AC. Using the TiO_2/RGO mixture with an RGO concentration of 5%, the degradation efficiency of 2 mg/mL AC in drinking water was about 71.29%.

Chapter 8 presents information on the synthesis and optical properties of composites based on reduced graphene oxide and poly-5amino-1-naphthol. These composites may have possible applications in the realization of a platform/sensor for the detection of the concentration of antipyretic drugs. The analysis of the RGO/P5A1N composites obtained by mechano-chemical interaction, but also by electropolymerization of 5A1N on the Au electrode covered with RGO sheets, revealed several details:

• Raman scattering and IR spectroscopy were used to demonstrate a chemical interaction between 5A1N and RGO sheets was demonstrated. This was justified by the presence of Raman lines at 1466 and 1620 cm^{-1} attesting the interaction of 5A1N with RGO and by the appearance of IR bands with maxima at 1670 and 3626–3726 cm^{-1}.

• The electrochemical polymerization reaction of 5A1N in the presence of $HClO_4$ and $H_4SiW_{12}O_{40}$ on the Au electrode covered with RGO layers leads to the covalent functionalization of RGO with P5A1N doped with $H_4SiW_{12}O_{40}$ heteropolyanions. And in this case, the choice of the

heteropolyanion $H_4SiW_{12}O_{40}$ was made taking into account its less oxidative properties, compared to other compounds.

Raman scattering studies and IR spectroscopy showed that: i) the presence of the R-NH-R functional group, is a consequence of the covalent functionalization of the RGO sheets with P5A1N, highlighted by the IR band at 3742 cm^{-1}; and (ii) the shift of the IR bands attributed to the naphthalene ring bending, the C–O bond stretching vibrational modes of phenolic compounds overlapping the in-plane bending of the O–H bond and the C=N bond stretching is a consequence of the covalent bonding of P5A1N in the doped state on the surface of the RGO sheets; (iii) the voltammograms recorded for the Au electrode and the Au electrode covered with RGO sheets showed an increase in current densities as the concentration of 5A1N was increased. This fact indicates a dependence of the reaction rate on the 5A1N concentration.

Novelties

The novelty of the experimental studies reported in this doctoral thesis consists in:

- demonstrating that photoluminescence can be an alternative optical method to UV-VIS spectroscopy for highlighting the photodegradation processes of pharmaceutical compounds;

- to explain the photodegradation processes of paracetamol and aspirin type drugs through correlated studies of UV-VIS spectroscopy, photoluminescence, FTIR spectroscopy and Raman scattering;

- improving the efficiency of removing traces of paracetamol-type drugs from polluted waters, by using composites based on reduced graphene oxide (RGO) and TiO_2 with anatase and rutile crystalline structures;

- the electrochemical synthesis of the RGO/P5A1N (poly-5-amino-1naphthol) composite and the understanding of the optical properties by performing correlated Raman scattering studies, FTIR spectroscopy, atomic force microscopy.

Future perspectives

The next step willbe to extend the research of this thesis,which aims to use the P5A1N/RGO composite to modify the surface of screen-printed electrodes, in order to create new electrochemical sensors for detecting drug concentrations in water samples contaminated with this type of compound.

List of works published in the doctoral thesis

1. **Dăescu M**, Matea A, Negrila C, Serbschi C, Ion AC, Baibarac M., *Photoluminescence as a Valuable Tool in the Optical Characterization of Acetaminophen and the Monitoring of Its Photodegradation* Reactions. Molecules, 2020, 25 (19), 4571.

F: 3.267 AIS : 0.599

2. Baibarac M, **Dăescu M**, Socol M, Bartha C, Negrila C, Fejer SN. *Influence of Reduced Graphene Oxide on the Electropolymerization of 5-amino-1-naphthol and the Interaction of 1, 4-phenylene Diisothiocyanate with the Poly (5-amino-1-naphtol)/Reduced Graphene Oxide Composite*., Polymers (Basel). 2020 Jun 5;12 (6):1299.

F: 3.426 AIS: 0.545

3. **Dăescu M**, Iota M, Serbschi C, Ion AC, Baibarac M. The Influence of UV Light on Photodegradation of Acetylsalicylic Acid, *International Journal of Molecular Sciences*, 2021, 22(8):4046.

F: 4.556 AIS: 0.943

4. **Dăescu M**, Chivu M, Matei E, Negrila C, Cramariuc O, Baibarac M. Photocatalytic Activity of the Blends Based on TiO_2 Nanoparticles and Reduced Graphene Oxide for Degradation of Acetaminophen. Molecules. 2023 Jun 4;28(11):4546.

F: 4.6 AIS :0.659

5. Alina Catrinel Ion, Mihnea Mlak-Marginean, Mihaela Savin, Monica Dăescu, Ion Ion, The influence of the aqueous composition over degradation of hydroxychloroquine, Buletinul UPB, 2022.

F:0.5 AIS:0.044

FI cumulat = 15.849

Patent

Chemical process for the assembly of poly(5-amino-1-naphthol) functionalised with graphene oxide based sensors for the detection of epidermal growth factor receptor/Procedeu chimic de asamblare a senzorilor bazati pe oxid de grafena functionalizati cu poli(5-amino-1-naftol) pentru detectia receptorului factorului de crestere epidermal, Dinescu Monica, Udrescu Adelina, Baibarac Mihaela, Fejer Szilard, A00691/02.11.2020

Oral communications at national workshops

1. **M. Dăescu,** M. Baibarac, M. Chivu, Fotodegradarea acetaminofenolului în prezența compozitelor bazate pe particule de TiO_2 si oxid de grafenă redus, Workshopul a prezentat rezultate obtinute in cadrul subcontractelor de tip D a proiectului AMD-FARMA-MED-RO, 3 Martie 2023, Măgurele, România, (Prezentare orală).

2. **Dăescu M**, Oprica M., Iota M., Fejer S.N., Negrila C., Baibarac M., Fotodegradarea atorvastatinei evidentiata prin studii de fotoluminescenta, Workshopul a prezentat rezultate obtinute in cadrul subcontractelor de tip D a proiectului AMD-FARMA-MED-RO, 30 Septembrie 2021, Măgurele, România, (Prezentare orală).

3. **Dăescu M**., Iota M., Serbschi C., Ion A. C., Baibarac M., Influenta lumnii UV asupra fotodegradrii acidului acetilsalicilic, Workshopul a prezentat rezultate obtinute in cadrul subcontractelor de tip D a proiectului AMD-FARMA-MED-RO, 30 Septembrie 2021, Măgurele, România, (Prezentare orală).

4. **Dăescu M**, Socol M., Bartha C., Fejer S.N., Negrila C., Baibarac M., Compozite bazate pe poli5amino-1naftol si oxid de grafena in stare redusa, Workshopul a prezentat rezultate obtinute in cadrul subcontractelor de tip D a proiectului AMD-FARMA-MED-RO, 30 Septembrie 2020, Măgurele, România, (Prezentare orală).

Conferences

Monica D., Mirela P., Stefania F., A. Udrescu, N'ghaya T., Radu C., Alina C. I., Ion I., Mihaela B., Applications of photoluminescence over the photodegradation of organic compounds, 22nd

Romanian International Conference on Chemistry and Chemical Engineering (RICCCE), Sinaia, 7-9 Septembrie, 2022.

Other works published during the doctoral internship

1. M. Paraschiv, **M. Dăescu**, C. Bartha, B. Chiricuta, M. Baibarac, Photodegradation of nifedipine highlighted by correlated studies of UV-VIS spectroscopy, photoluminescence, Raman scattering, FTIR spectroscopy, thermogravimetry and mass spectrometry, Pharmaceuticals, 2023.
2. Cercel R, Paraschiv M, Florica CS, **Dăescu M**, Udrescu A, Ciobanu RC, Schreiner C, Baibarac M. New Aspects Concerning the Ampicillin Photodegradation. Pharmaceuticals. 2022; 15(4):415.
3. Bărbatu A., Lungan M. A., N'ghaya T., Smaranda I., **Dăescu M**., Baibarac M., Manta C. M., Physico-chemical properties of two anhydrous azathioprine forms and their interaction with typical pharmaceutical excipients: highlighting new findings in drug formulation development, Drug Development and Industrial Pharmacy, 2021, 47:10, 1598-1606.
4. Baibarac M, **Dăescu M**, Matei E, Nastac D, Cramariuc O. Optical Properties of Composites Based on Poly(o-phenylenediamine), Poly(vinylenefluoride) and Double-Wall Carbon Nanotubes. International Journal of Molecular Sciences. 2021; 22(15):8260.
5. Smaranda I, Nila A, Ganea P, **Dăescu M**, Zgura I, Ciobanu RC, Trandabat A, Baibarac M. The Influence of the Ceramic Nanoparticles on the Thermoplastic Polymers Matrix: Their Structural, Optical, and Conductive Properties. Polymers. 2021; 13(16):2773.
6. Oprica M, Iota M, **Dăescu M**, Fejer SN, Negrila C, Baibarac M. Spectroscopic studies on photodegradation of atorvastatin calcium. International Journal of Molecular Sciences. 2021, 28;11(1):15338.
7. Baibarac M., **Dăescu M**, Fejer SN. Optical Evidence for the Assembly of Sensors Based on Reduced Graphene Oxide and Polydiphenylamine for the Detection of Epidermal Growth Factor Receptor. Coatings. 2021; 11(2):258.
8. Baibarac M, Arzumanyan G, **Dăescu M**, Udrescu A, Mamatkulov K. Anisotropic Photoluminescence of Poly (3-hexyl thiophene) and Their Composites with Single-Walled Carbon Nanotubes Highly Separated in Metallic and Semiconducting Tubes. Molecules. 2021; 26(2):294.
9. Toulbe N, Stroe MS, **Dăescu M**, Cercel R, Mogos A, Dragoman D, Socol M, Mercioniu I, Baibarac M. Reduced Graphene Oxide Sheets as Inhibitors of the Photochemical Reactions of α-Lipoic Acid in the Presence of Ag and Au Nanoparticles. Nanomaterials. 2020; 10(11):2238.
10. **Dăescu M**, Toulbe N, Baibarac M, Mogos A, Lőrinczi A, Logofatu C. Photoluminescence as a Complementary Tool for UV-VIS Spectroscopy to Highlight the Photodegradation of Drugs: A Case Study on Melatonin. Molecules. 2020; 25(17):3820.

The present abstract contains in a concise form the content of the original contributions specific to chapters 5-8, and the numbering of chapters, sub-chapters, tables, figures, diagrams and selective references corresponds to that in the thesis.

Selective bibliography:

[205] J. J. Thiessen, "Aspirin: Plasma concentration and effects," *Thromb. Res.*, vol. 29, pp. 105–111, Jan. 1983, doi: 10.1016/0049-3848(83)90365-1.
[215] [1] S. Eigler, C. Dotzer, and A. Hirsch, "Visualization of defect densities in reduced graphene oxide," *Carbon N. Y.*, vol. 50, no. 10, pp. 3666–3673, Aug. 2012, doi: 10.1016/j.carbon.2012.03.039.

[218] P. D. J. Rubio, J. L. Oteo, M. Villegas, “Characterization and sintering behaviour of submicrometre titanium dioxide spherical particles obtained by gas-phase hydrolysis of titanium tetrabutoxide,” *J. Mater. Sci.*, vol. 32, pp. 643–652, 1997, doi: 10.1023/A:1018579500691.
[229] S. Ahmad, M. Almehmadi, H.T. Janjuhah, G. Kontakiotis, O. Abdulaziz, K. Saeed K, H. Ahmad, M. Allahyani, A. Aljuaid, A. A. Alsaiari, Mazen Almehmadi, H. T. Janjuhah, G. Osama Abdulaziz, J. Muhammad, I. Khan, “The Effect of Mineral Ions Present in Tap Water on Photodegradation of Organic Pollutants: Future Perspectives,” *Water*, vol. 15, no. 1, p. 175, Jan. 2023, doi: 10.3390/w15010175
[232] R. M. Silverstein and G. C. Bassler, “Spectrometric identification of organic compounds,” *J. Chem. Educ.*, vol. 39, no. 11, p. 546, Nov. 1962, doi: 10.1021/ed039p546.